BENEMERITA UNIVERSIDAD AUTÓNOMA DE PUEBLA

Facultad de Ciencias Físico Matemáticas

Photoproduction of $\pi^+\pi^-$ and $\pi^+\pi^-\pi^+\pi^-$ in lead-lead collisions at ALICE-LHC.

TESIS

Presentada para obtener el título de
Maestría en Ciencias Física Aplicada

Presenta
Sergio Paisano Guzmán

Diector de Tesis: Dr. Mario Rodríguez Cahuantzi

Puebla, Pue. Diciembre 2020

BENEMERITA UNIVERSIDAD AUTÓNOMA DE PUEBLA

Abstract

Facultad de Ciencias Físico Matemáticas
Cuerpo académico: Física de Partículas Elememntales

Maestría en Física Aplicada

Photoproduction of $\pi^+\pi^-$ and $\pi^+\pi^-\pi^+\pi^-$ in lead-lead collisions at ALICE-LHC.

by Sergio Paisano Guzmán

The ALICE experiment at CERN LHC was designed to study heavy ion collisions as well as proton collisions. Electromagnetic interactions are present in such collisions; The electromagnetic field of a charged particle moving at ultrarelativistic velocities can be considered as a photon cloud that surrounds the particle. The photon cloud of a projectile nucleus can interact with the entire target nucleus, its constituents or its photon cloud, giving as result the production of new particles. To distinguish these processes from hadronic processes a condition in the impact parameter is required, it must be bigger than the raddi sum of colliding particles. Collisions that met this requirement are called ultraperipheral.

The study of $\pi^+\pi^-$ and $\pi^+\pi^-\pi^+\pi^-$ photoproduction at ALICE in ultraperiperipheral Pb-Pb collisions at $\sqrt{S_{NN}} = 5.02TeV$ during 2018 and Xe-Xe collisions at $\sqrt{S_{NN}} = 5.44TeV$ during 2017 is presented.

Acknowledgements

Quiero agradecer a mis padres por el apoyo brindado durante toda mi vida.

Al Dr. Mario Rodríguez Cahuantzi por su apoyo durante la realización de este trabajo de tesis.

Al Consejo Nacional de Ciencia y Tecnología (CONACYT) por el apoyo económico brindado.

Al Consejo de Ciencia y Tecnología del Estado de Puebla (CONCYTEP) por su apoyo otorgado para la realización de una estancia en la Organización Europea para la Investigación Nuclear(CERN), a traves del Convenio Número: 104/2020.

Este trabajo fue parcialmente financiado por CONACYT a través del proyecto Conacyt CB A1-S-13525.

...

Contents

List of Figures

List of Tables

Chapter 1

Introduction

ALICE(A Large Ion Collider Experiment) is a major experiment at the Large Hadron Collider (LHC), Geneva, which is optimized for the study of QCD matter created in high-energy collisions between lead nuclei, though additional studies can be carried out due to the great capabilities of triggering and tracking of the detectors in ALICE. One of such studies are the ultraperipheral collisions in which particles do not interact hadronically, the interaction occurs through the electromagnetic field that surrounds them. This thesis focuses on the coherent production of $\pi^+\pi^-$ and $\pi^+\pi^-\pi^+\pi^-$ in lead-lead UPC at $\sqrt{S_{NN}} = 5.02TeV$.

The First chapter corresponds to the introduction of the thesis.

In the second chapter, a brief historic introduction about particle physics is given, and also the main variables used in particle physics are presented .

In the second chapter, the Ultraperipheral collisions are presented from a theoretical point of view. Main works in particles photoproduction related to this thesis work are also presented and briefly explained in this chapter.

The third chapter includes the description of the ALICE experiment detectors and trigger systems. Also a brief explanation of the computational resources of the ALICE experiment is presented.

The main work carried out during this thesis work is presented in chapter 4. In this chapter the detailed selection of events and analysis of physical observable is presented. The simulated events events used to determine the acceptance and efficiency corrections for the data sample are included in this chapter. Corrected for acceptance and efficiency invariant mass distributions for the 2 and 4 pins data samples are presented in this chapter.

The final chapter are the conclusions, this chapter summarize the main results obtained from the data analysis and also list some of the future work need to be developed in order to obtain a value for the cross sections in the 2 an 4 cases.

Chapter 2

Particle Physics

The concept of matter being composed by elementary particles arise around 2500 years ago, when Greek philosophers, Democritus and Leucippus, proposed that all matter is made up of bonding atoms. However, it was not until 1987 with the discovery of the electron, achieved by J.J. Thomson, when particle physics was formally started,aimed to the study of matter from a fundamental point of view. Thompson realised that cathodic rays emitted by a hot filament could be deviated by the presence of a magnetic field, this suggested that cathodic rays were not rays at all, rather a current of charged particles; besides, due to the direction of the curvature, such particles should have negative charge. When the beam passed through both magnetic and electric fields, which had been adjusted in such a way that the deviation of the beam was zero, Thomson was able to measure the charge-mass relation of the particles, in this way he concluded that either the mass was little or the charge was huge. The first option was the one that agreed with the experiments, after this, the discovered particles were named *electrons*.

Thomson thought that electrons were part of the atom, nevertheless, atoms are electrically neutral and thousand of times heavier than electrons. Hence, Thomson proposed his known atomic model, in which electrons are held by a positively charged dense material, such as plums located in a pudding. This model was discarded by the Rutherford's scattering experiment, showing that the atom is almost empty, it contains a very small nucleus with positive charge and the largest amount of mass.

In 1914, Niels Bohr suggested his atomic model for the hydrogen atom, where the proton is surrounded by a unique electron, similar to a planet moving around a star. The estimations of the Bohr model for the hydrogen spectrum were consistent with the experiments, supporting the fact that the heavier atoms consisted of a certain number of bonded protons in order to maintain a neutral charge, though, difficulties with this supposition arose when considering the next heavier elements; for instance, Helium and Lithium (with two and three electrons, respectively) are two and seven times heavier than hydrogen. Such problem was solved in 1932 when Chadwick discovered the neutron. Neutrons, as the name suggests, are electrically neutral. What is more, in terms of mass, neutrons can be considered as the proton twin. The number of neutrons in the atom is not necessarily the same as the number of protons, this variations result into *isotopes*, which are those elements with the same number of electrons and protons, but a different number of neutrons. One of the most

common examples of this type of atoms, are the Hydrogen isotopes: Protium (0 neutrons), Deuterium (1 neutron), and Tritium (2 neutrons).

Up to this point in history, it could be thought that the end had been reached in understanding the fundamental structure of matter. Everything that can be seen, touched and smelt is made of protons, neutrons, and electrons. But this idea did not last long. A new question arose: what holds the protons together in the nucleus? Protons should repel each other due to their electrical nature, and neutrons have no apparent reason to stay there; undoubtedly there should be a force that holds the nucleus together, one stronger than the electrical force, which in this case would be repulsive. This new force was called *strong force*. A special feature of this force is that its effects are only considerable over a very short distance range, unlike electromagnetic and gravitational forces, both of which have an infinite distance range, despite the fact that they could be negligible at a finite distance. The range of the strong force is approximately the size of the core itself; that is the reason why atoms with a large number of protons in their nucleus tend to be unstable.

In 1934 Yukawa proposed a theory of the strong force in which protons and neutrons are attracted to each other by some kind of force, and of a particle whose exchange accounts for the characteristics of the strong force. Yukawa stated that the mass of this particle should be about one third of the mass of the proton; since this mass value is between the mass of the proton and the mass of the electron, the particle was named *meson*, which means "Middleweight". At that time there was a lack of experimental evidence for such particle. It was in 1937 when, thanks to a cosmic ray experiment, hints of the Yukawa meson were obtained. Unfortunately, later experiments, also with cosmic rays, showed that the Yukawa meson was actually a particle produced in the upper atmosphere due to the interaction of cosmic rays with air molecules, and that it has nothing to do with strong interactions. This new particle was discovered in 1947 and received the name of pion (π), it was discovered at the same time as another particle of "medium weight", the muon (μ), also produced by cosmic rays. Thanks to these discoveries, a new stage in the understanding of matter began, originating studies of the physics of particles. The work of theoretical and experimental physicists resulted in what is now known as the *Standard Model of fundamental particles*.

2.1 The Standard Model

The Standard Model is considered one of the most successful theories in physics, since it manages to describe, with a good approximation, the interactions of fundamental particles. As a result, there is a study of three of the elemental forces of nature: the electromagnetic force, the weak force and the strong force. It is said that a particle is fundamental when it does not have an internal structure, that is, a fundamental particle is punctual.

The Standard Model establishes that all known matter in the Universe is made up of fermions, which are particles with half-integer spin, which interact through the mediators of forces, also known as bosons, these are particles with integer spin. In turn, fermions are divided into quarks and leptons. The former

are characterized by having a charge of color, which allows them to interact with the strong force; the mediators of this force are gluons (g). In the case of leptons, some have an electric charge (e, μ, τ), and others do not (ν_e, ν_μ, ν_τ), as it can be seen in the figure 2.1, so the electromagnetic and weak forces can act on quarks and leptons. Neutrinos, on the other hand, having no electrical charge, do not feel the electromagnetic force, but they do feel the weak force.

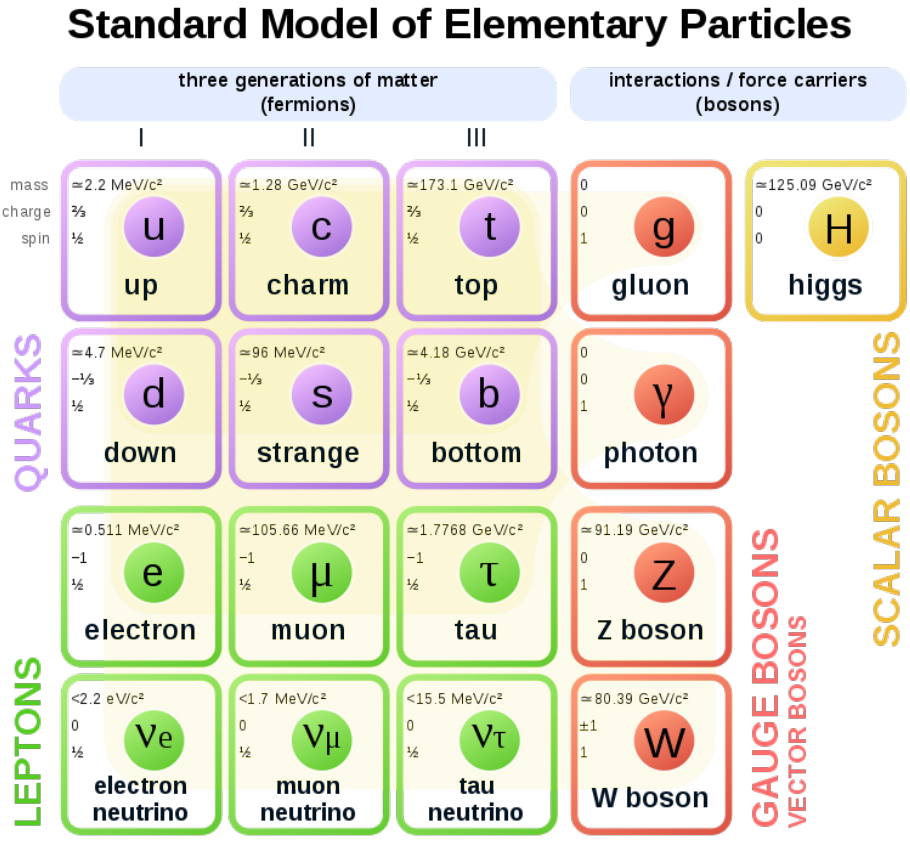

FIGURE 2.1: Standard Model of particle physics

The mediating particle of the electromagnetic force is the photon (γ), and those of the weak force are the bosons $W^{\pm}$, Z. These mediators (together with the gluons g) are called vector bosons since their spin is one, although there are also scalar bosons, which have zero spin. The Higgs boson (a scalar boson) was the last remaining particle to be observed in order to verify that this model is correct. It was in 2012 when the LHC, ATLAS and CMS experiments found signals of a particle with the properties of the boson proposed in the Standard Model, verifying the validity of the theory.

One of the biggest success of the Standard Model is the proposal of a process for the mass generation of the particles, known as Higgs-Englert-Brout mechanism. This process is possible through the spontaneous symmetry breaking (SSB), where a field associated to a particle acquires mass ([**COTT**]). Due to observations detected by the ATLAS and CMS experiments at CERN, Peter Higgs and Francois Englert were awarded with the Nobel Prize in Physics in 2013.

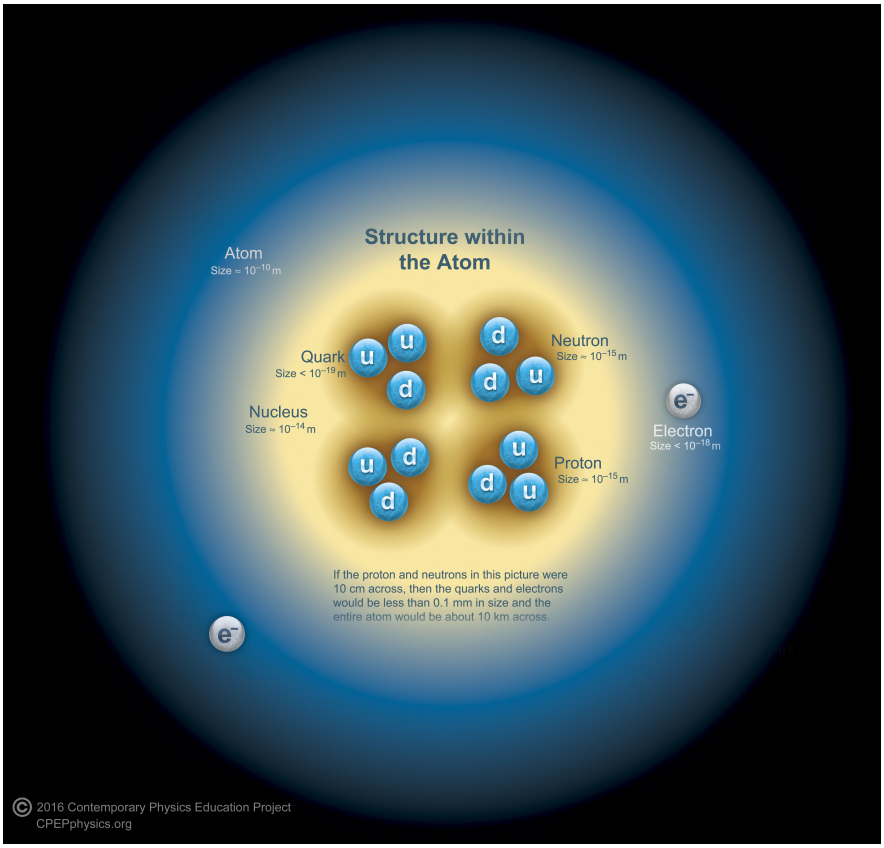

FIGURE 2.2: Structure within the atom [22]

Quarks and leptons can be classified in *generations*, as it can be seen in Figure 2.1. Those particles belonging to the first generation are lighter than those in the second generation; in the same way, the particles of the second generation have fewer mass than the particles of the third generation. In Figure 2.2 it can be seen how most of the known matter is made of fermions of the first generation: quark up (u) and quark down (d), the electron (e) and the electron neutrino (ν_e).

Even though many of the predictions of the Standard Model have been proved, there are evidences that the model is unable to explain some processes. For instance, it is incapable to include gravity, as well as the origin of the coupling constants or the mass hierarchy. In the Standard Model neutrinos are considered to be massless, however current experiments indicate the opposite, actually intervals of the mass range are given for their mass (such mass is very small compared with the other particles since it is in the order of 2 MeV).

These and more problems have been found in the Standard Model, for this reason it is important to analyse the basis of the theory with the help of experimental data. One of the most studied fields in particle physics, used in order to search solutions to such problems, is the quantum chromodynamics, which is the topic of the next section.

2.2 Quantum chromodynamics

Quantum Chromodynamics (QCD by its initials) is a gauge theory which describes the strong interactions between quarks. Due to the fact that quarks have *color charge*, they can interact through the mediators of the strong force, the gluons.

A combination of quarks forms structures called *hadrons*, such as the proton and the neutron. A system containing three quarks constitutes a *baryon*, in the other hand, a particle with a quark and an antiquark results into a *meson*. Each flavor has associated three color charges, hence it is possible to represent a quark as a color triplet:

$$\mathbf{u} = \begin{pmatrix} u_r \\ u_g \\ u_b \end{pmatrix} \tag{2.1}$$

Where suffixes denote the color charge: u_r corresponds to a red color, u_g to a green color, and u_b to a blue color charge. It is known that quarks composing a hadron are confined, since it is infeasible to detect them individually, as well as gluons. Figure 2.3 shows a fundamental process in QCD

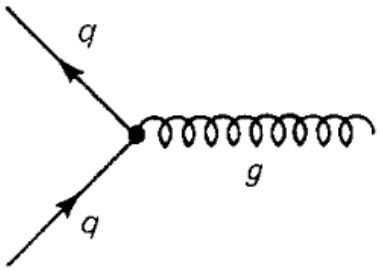

FIGURE 2.3: Feynman diagram for a $q \rightarrow q + g$ process, taking the time evolution upward [31]

Regarding the previous process, the color of the quarks could change, whereas the flavour is conserved; although, the final color charge has to be conserved too. For example, if the quark down has a blue charge, at the end of the process it can have a green charge, hence the gluon has a green and an anti-blue color charges. Gluons have a double charge color, one positive and one negative. There are eight possible combinations for the color charge of a gluon.

Due to the fact that gluons have color charge, it is possible to have self-interactions among them, as it is shown in figure 2.4. There are *coupling constants* for each type of interaction, as the name suggests, determine the strength of the interaction between particles or fields. The value of such constants depends on the energy scale, i.e., on the distance from one particle to the other. Figure 2.5 shows the evolution of the QCD constant coupling α_s, which has *asymptotic freedom*. This means that, when the distance between quarks is very small (such as inside a hadron) the interaction force will have a small

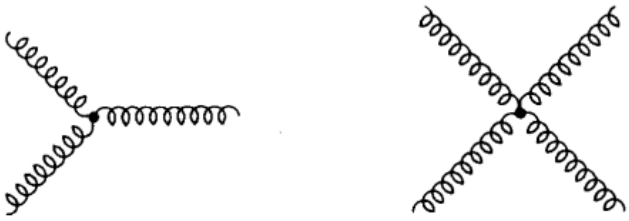

FIGURE 2.4: Feynman diagram for two gluon sel-interations processes ([31])

value, too. Quarks move freely, since any force is strong enough to keep them bonded.

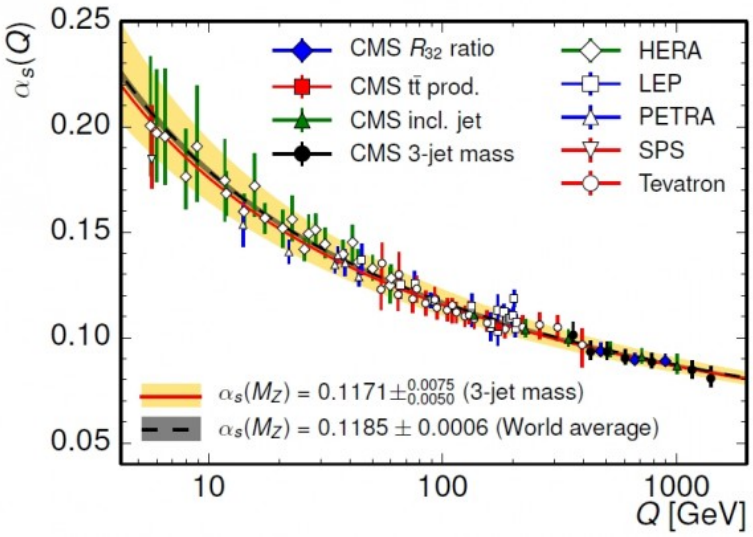

FIGURE 2.5: α_s experimental values [14]

It is expected to understand the nature of quarks through the study of hadrons. Protons are one of the main particles analysed, hence a description of them is given in the following section.

2.3 Pions

Unlike protons, pions (π) are mesons, which means they are composed by a quark (q) and an antiquark ($\bar{q}$). These type of particles are the lightest mesons. Pions can have positive charge (π^+), negative charge (π^-), and neutral charge (π^0), depending on their composition, as it can be seen in Table 2.1.

Pions are mostly created at hadron colliders, they are also produced naturally, for example when cosmic rays interact with matter in Earth's atmosphere. The pions lifetime is approximately 2.6×10^{-8}s. Depending on the content of a pion, it can decay to different particles [4], as it is shown in Table 2.2, where the decay rates are included.

TABLE 2.1: Quark composition of Pions

Pion	Composition
π^+	$u\bar{d}$
π^-	$d\bar{u}$
π^0	$u\bar{u}$, $d\bar{d}$

TABLE 2.2: Pion decays

Decay	Rate
$\pi^+ \to \mu^+\nu_\mu$	99.98%
$\pi^+ \to \mu^+\nu_\mu\gamma$	1.2×10^{-4}%
$\pi^- \to \mu^-\bar{\nu}_\mu$	99.98%
$\pi^- \to \mu^-\bar{\nu}_\mu\gamma$	1.2×10^{-4}%
$\pi^0 \to \gamma\gamma$	98.82%
$\pi^0 \to e^+e^-\gamma$	1.17%

2.4 Kinematics

In particle physics there are certain quantities necessary for the description of scattering processes, some of them are listed below:

2.4.1 Rapidity

The rapidity and pseudorapidity (see section 2.4.2) are 2 variables commonly used in particle accelerators, which arose because the velocities of the incident particles, or at least most of its magnitude, are directed along the beam axis. In collision experiments usually the beam axis coincides with the z axis, as shown in the figure 2.6:

In such reference system the rapidity "y" is defined as [23]:

$$y = \frac{1}{2}\ln\left(\frac{E + p_z c}{E - p_z c}\right) \tag{2.2}$$

where E is the particle energy, p_z is its momentum in the z direction and c is the light velocity. In high-energy collisions, the rapidity gives us information about the angle at which the particles are emitted after a collision, for example, if the rapidity were zero or approximately zero, it would imply that $(E + p_z c)/(E - p_z c) \approx 1$ and so $p_z \approx 0$ which would indicate that the emitted particle came out in a direction practically perpendicular to the axis of the beam, on the other hand, if the rapidity had an outsize magnitude($y \approx \infty$) then, $(E + p_z c)/(E - p_z c) \approx \infty$ and $E \approx p_z c$, so the particle emitted in this case would come out in a direction almost parallel to the beam axis, and finally if

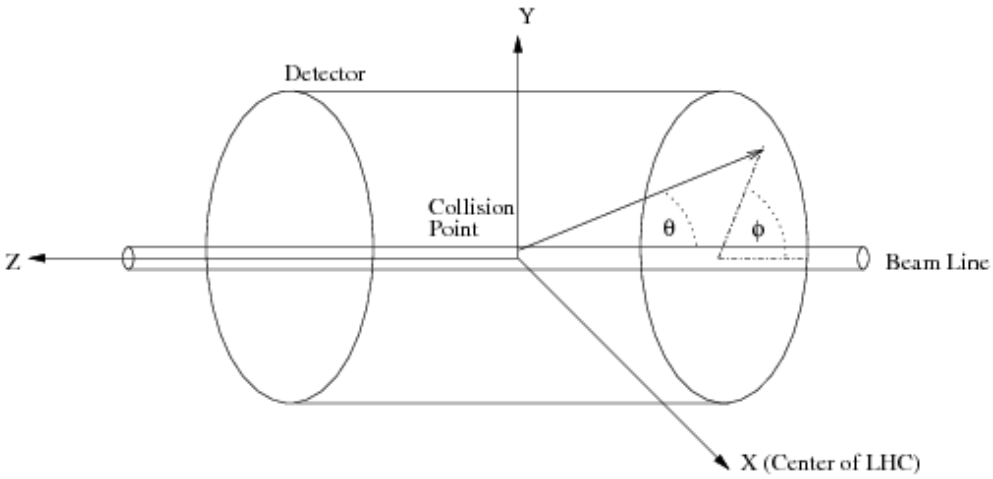

FIGURE 2.6: Reference System in particle collision experiments

$y \approx -\infty$ the particle would also come out with an angle almost equal to zero with respect to the beam axis, but at opposite direction.

If we consider a reference frame S' moving at a velocity v in the direction of the z axis with respect to a reference frame S, the rapidity in the frame S' will be defined as:

$$y' = \frac{1}{2}\ln\left(\frac{E' + p'_z c}{E' - p'_z c}\right) \tag{2.3}$$

The energy E and the moment **p** in the system S are related to the energy E 'and the moment textbf p' of the system S' as follows:

$$E' = \frac{E - v p_x}{\sqrt{1 - \frac{v^2}{c^2}}} \quad p'_x = p_x \quad p'_y = p_y \quad p'_z = \frac{p_z - \frac{Ev}{c^2}}{\sqrt{1 - \frac{v^2}{c^2}}} \tag{2.4}$$

According to the equations 2.4 the transformation of the rapidity from the reference frame S' to the frame S is:

$$y' = y + \frac{1}{2}\ln\left(\frac{1 - \frac{v}{c}}{1 + \frac{v}{c}}\right) \tag{2.5}$$

If in a collision two particles are generated, each one with rapidity y'_1 and y'_2, we can note that the rapidity difference measured is independent of the reference system used; according to 2.5

$$y'_2 - y'_1 = y_2 + \frac{1}{2}\ln\left(\frac{1 - \frac{v}{c}}{1 + \frac{v}{c}}\right) - y_1 - \frac{1}{2}\ln\left(\frac{1 - \frac{v}{c}}{1 + \frac{v}{c}}\right)) = y_1 - y_2 \tag{2.6}$$

2.4.2 Pseudorapidity

As already explained, rapidity is very useful if the moment and energy of the particle are known, however in collisions where the energy is very large, these

quantities, especially the moment, are difficult to measure, so it is convenient to define a new variable similar to rapidity but easier to measure. This new variable is called pseudorapidity and is denoted by the symbol η. We can obtain the pseudorapidity from the expression for the rapidity given by 2.2, considering $E^2 = \mathbf{p}^2c^2 + m^2c^4$:

$$y = \frac{1}{2}\ln\left(\frac{\sqrt{\mathbf{p}^2c^2 + m^2c^4} + p_z c}{\sqrt{\mathbf{p}^2c^2 + m^2c^4} - p_z c}\right) \tag{2.7}$$

For relativistic particles with very high energy $p^2c^2 >> m^2c^4$. Factoring pc in each square root in 2.7 and using the binomial expansion, we found the following approximation.

$$y \approx \frac{1}{2}\ln\left(\frac{1 + \frac{p_z}{\mathbf{p}}}{1 - \frac{p_z}{\mathbf{p}}}\right) \tag{2.8}$$

The angle between the beam axis and the direction of the emitted particle is defined as $\theta = \arccos(p_z/\mathbf{p})$, therefore $1 + p_z/\mathbf{p} = 2\cos^2(\theta/2)$ and $1 - p_z/\mathbf{p} = 2\sin^2(\theta/2)$, substituting this into 2.8 we have:

$$y \approx -\ln\left(\tan\frac{\theta}{2}\right) \tag{2.9}$$

The pseudorapidity is defined as:

$$\eta = -\ln\left(\tan\frac{\theta}{2}\right)$$

For highly energetic particles, in which $E \approx p$, the rapidity is approximately equal to the pseudorapidity ($y \approx \eta$). In figure 2.7, the relation between the polar angle θ and the pseudorapidity η can be seen. In the rest of this chapter,natural units in which the speed of light $c = 1$ will be used.

2.4.3 Mandelstam Variables

Mandesltam variables are lorentz invariants, which are used to describe the kinematic of scattering processes of type $1 + 2 \to 3 + 4$, an schematic example of these processes is observed in figure 2.8, in which two incident particles 1 and 2, with 4-momenta p_1 and p_2 respectively, interact and become particles 3 and 4 with 4-momenta p_3 and p_4.

There are 3 Mandelstam variables, labelled with the letters s, t, u and are defined as:

$$s = (p_1 + p_2)^2 = (p_3 + p_4)^2 \tag{2.10}$$

$$t = (p_1 - p_3)^2 = (p_4 - p_2)^2 \tag{2.11}$$

$$u = (p_1 - p_4)^2 = (p_3 - p_2)^2 \tag{2.12}$$

where p_1 and p_2 are the 4-momenta of the incident particles and p_3 y p_4 the 4-moment of the outgoing particles.

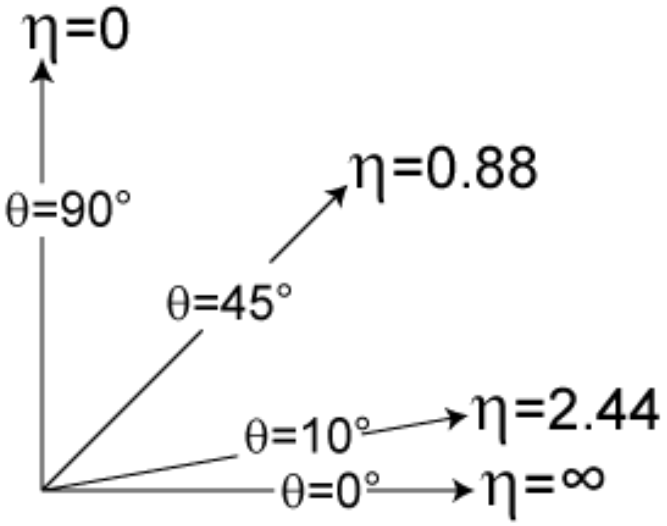

FIGURE 2.7: Relación entre el ángulo polar θ y la pseudorapidez η

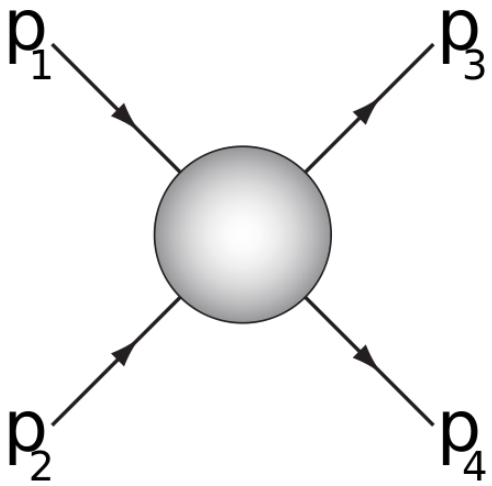

FIGURE 2.8: Proceso de dispersión de 2 cuerpos: $1 + 2 \rightarrow 3 + 4$

The 4-momenta conservation applied to the process shown in figure 2.8 gives:

$$p_1 + p_2 - p_3 - p_4 = 0 \tag{2.13}$$

which leads to:

$$s + t + u = m_1^2 + m_2^2 + m_3^2 + m_4^2 \tag{2.14}$$

From expression 2.14 is clear that only 2 of the 3 Mandelstam variables are independent, besides the sum of the 3 is a constant given by the sum of the squared masses of the 4 particles involved in the process. Considering the center of mass frame where $p_1 - p_2 = p_3 - p_4 = 0$ and recalling that 4-momenta of a particle wilt mass m is given by $p^\mu = (E, \mathbf{p})$:

$$p_\mu p^\mu = p^2 = E^2 - \mathbf{p}^2 = m^2 \tag{2.15}$$

where E is the particle energy and $\mathbf{p} = (p_x, p_y, p_z)$ its momentum. Mandelstam variables can be written as follows:

$$s = (E_1 + E_2)^2 = (E_3 + E_4)^2 \tag{2.16}$$

$$t = m_1^2 + m_3^2 - 2(E_1 E_3 - |\mathbf{p}_1|\,|\mathbf{p}_3| \cos\theta) \tag{2.17}$$

$$u = m_1^2 + m_4^2 - 2(E_1 E_4 + |\mathbf{p}_1|\,|\mathbf{p}_3| \cos\theta) \tag{2.18}$$

In the equations 2.17 and2.18, θ is the angle of scattering between incident particle 1 and outgoing particle 3. According to 2.16, the variable s is the total energy squared, measured from the center of mass frame, while the variable t is the squared momentum transferred.

Chapter 3

Ultraperipheral Collisions

An atom in its ground state can be taken to a excited state when it is irradiated with light of certain frequency; the atom energy raises due to the absorption of photons. Eventually the atom will return to its ground state through photons emission. On the other hand, a moving charged particle passing near a point p generates an electric field which changes over time at this point (and in the whole space), it can be shown that the electric field at this point is equivalent to light with certain frequency distribution passing through this point. And if an atom is placed at p a similar phenomena as the presented in the beginning will occur. This is known as the equivalent method of photons and was proposed by Fermi in 1924 [28]. Ten years later, Weizsacker and Williams resumed this idea and spread it to the ultrarelativistic case in what is known as the Weizsacker-Williams approximation[27].

The Ultraperipheral Collisions (UPC) are characterized due the impact parameter, it must be bigger than the radii sum of the colliding particles[1]. The hadronic interactions are highly suppressed. In UPC the particles interact through the photon cloud that surround each ion (see figure 3.1); due the electromagnetic field intensity has Z^2 dependence, the density of the photon cloud will also depend on this, therefore the probability to have interactions in heavy ion collisions is bigger in Pb-Pb collisions than in proton collisions where $Z = 1$.

Two type of interactions occur in general in UPC:

- Photon-Photon: The irradiated photons of both atoms interact with each other. Interactions between photons have been previously studied in colliders of photons such as HERA [11] and CERN LEP[43].
- Photonuclear: The irradiated Photons of an ion interact with the colliding ion. The photons can interact with the whole ion or with its constituents, so two different processes can be distinguished:
  - Coherent Process: The photon interact with the entire ion; the ion usually remain intact
  - Incoherent Process: The photon interact just with one nucleon; the ion usually breaks up and neutrons are emitted in forward direction.

Furtehrmore a photonuclear reaction in which a nuclei breaks up due to an additional photon exchange can occur. The interactions are schematized in figure 3.2

The UPC allow the study of three areas mainly: processes in quantum electrodynamics(QED) with strong electromagnetic fields, quantum chromodynamics (QCD) and new physics.

One of the main interests in photoproduction of vector mesons is the possibility to determine directly the gluon density in nucleons and nuclei[10]. The gluons distribution can be probed in production of heavy vector mesons, photoproduction of heavy quark-anti-quark pairs, and photoproduction of jets. As a first approximation, the nuclear gluon density can be written as the nucleon gluon distribution $g\left(x, Q^2\right)$ multiplied by the number of nucleons (A).

$$G^A\left(x, Q^2\right) = Ag\left(x, Q^2\right) \tag{3.1}$$

where, x, is the fraction of the projectile momentum carried by the gluon, and Q^2 is the 4-momentum transfer squared. Photoproduction at heavy-ion colliders may provide a more direct measurement of $G^A\left(x, Q^2\right)$.

The cross section for photoproduction of a state X is:

$$\sigma_X = \int d\omega \frac{n(\omega)}{\omega} \sigma_X^{\gamma}(\omega) \tag{3.2}$$

where σ_X^{γ} is the photonuclear cross section, and $n(\omega)$ is the number of photons with energy ω.

The cross section for two-photon processes is [9]:

$$\sigma_X = \int d\omega_1 d\omega_2 \frac{n\left(\omega_1\right)}{\omega_1} \frac{n\left(\omega_2\right)}{\omega_2} \sigma_X^{\gamma\gamma}\left(\omega_1, \omega_2\right) \tag{3.3}$$

where $\sigma_X^{\gamma\gamma}\left(\omega_1, \omega_2\right)$ is the two-photon cross section.

3.1 The photon flux

The flux of equivalent photons from a charged particle is determined from the Fourier transform of the electromagnetic field of the moving charge.

Let's consider two particles, a projectile and a target, with charge and mass numbers (Z_1, A_1) and (Z_2, A_2) respectively. Suppose the target particle is fixed in the origin of coordinate system, and assume the projectile particle moves in straight line parallel to the Z axis and with an impact parameter b. if the particle velocity is near c, the light velocity, the relativistic effect leads to a contraction of the electromagnetic field in its transverse components. The components of the time dependant electromagnetic field for a relativistic charged particle given by:

$$E_z = -Z_1 e \gamma v t / \left[b^2 + \gamma^2 v^2 t^2\right]^{3/2} \tag{3.4}$$

$$E_{\mathrm{T}} = -Z_1 e \gamma b / \left[b^2 + \gamma^2 v^2 t^2\right]^{3/2} \tag{3.5}$$

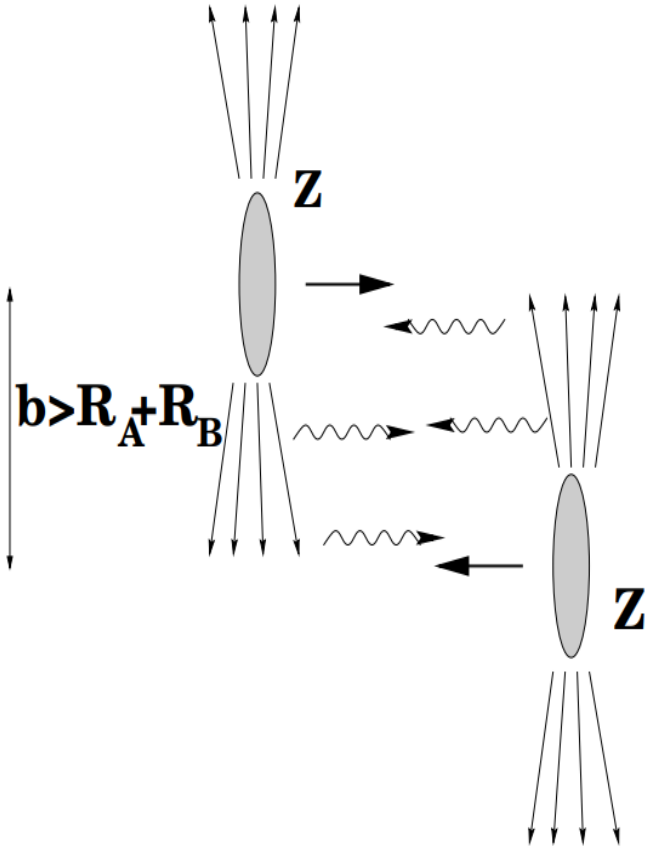

FIGURE 3.1: Schematic diagram of an ultraperipheral collision of two ions [1]

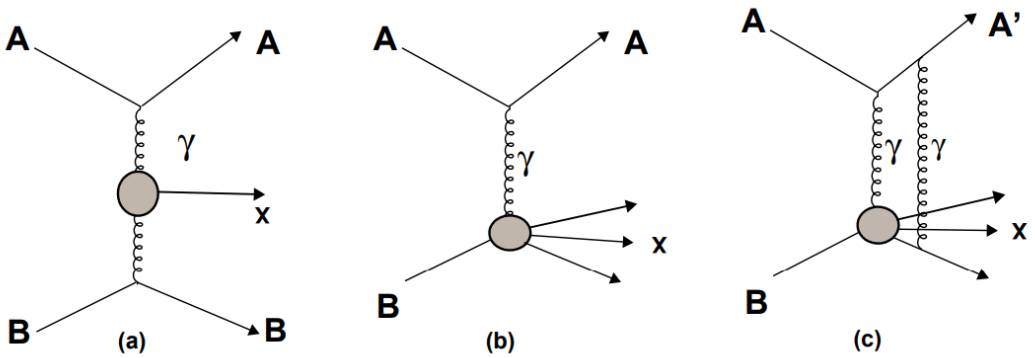

FIGURE 3.2: A schematic view of (a) Photon-Photon interaction, (b) a photonuclear reaction in which a photon emitted by an ion interacts with the other nucleus, (c) photonuclear reaction with nuclear breakup due to photon exchange [1]

$$B_{\mathrm{T}} = |v/c \times E_{\mathrm{T}}| \tag{3.6}$$

$$B_z = 0 \tag{3.7}$$

where γ is the Lorentz factor, z and T denote the transverse and longitudinal components of the electric and magnetic fields and b is the impact parameter.

if $v \approx c$, the transverse fields are equivalent to a pulse of plane polarized light as shown in figure 3.3, the longitudinal fields can be also treated as a pulse of light if a field B_z is introduced, this field does not affect the dynamics of the problem, since the electric field E_z (and so the pulse in that direction), are of minor relevance when $v \approx c$. Applying the Fourier transform on the time-varying fields E and B in Eqs(4.1-4.3), we can calculate the amount of energy incident on the target per unit area and per frequency interval:

$$I(\omega, b) = (\frac{c}{4\pi})|\boldsymbol{E}(\omega) \times \boldsymbol{B}(\omega)| \tag{3.8}$$

where $\boldsymbol{E}(\omega)$ and $\boldsymbol{B}(\omega)$ are the Fourier transforms of the Fields.

Considering the cross section $\sigma_\gamma(\hbar\omega)$ for an electromagnetic process generated by a pulse of equivalent light, the probability for the electromagnetic process to occur is:

$$P(b) = \int I(\omega, b)\sigma_\gamma(\hbar\omega)\mathrm{d}(\hbar\omega) = \int N(\omega, b)\sigma_\gamma(\omega)\frac{\mathrm{d}\omega}{\omega} \tag{3.9}$$

The integral runs over the full frequency spectrum of the virtual radiation. $N(\omega, b)$ is the number of equivalent photons incident on the target per unit area, and calulated from Eq 3.9 using Eq 3.8, can be expressed as:

$$N(\omega, b) = \frac{Z_1^2\alpha}{\pi^2}\left(\frac{\omega}{\gamma v}\right)^2\left(\frac{c}{v}\right)^2\left[K_1^2(x) + \frac{1}{\gamma^2}K_0^2(x)\right] \tag{3.10}$$

where K_0 and K_1 are modified Bessel functions and $x = \omega b/\gamma v$. The first term of 3.10 comes from the transverse pulse, while the second term comes from the longitudinal pulse, so is clear the longitudinal pulse contribution is negligible when $v \approx c \implies \gamma >> 1$.

The flux at an impact parameter b in 3.10 is related to the flux $n(\omega)$ in Eq 3.2 by $n(\omega) = \int 2\pi b N(\omega, b)db$. Integrating from b = R(the radii sum of the target and projectile) up to ∞ we get:

$$n(\omega) = \int_R^\pi 2\pi b N(\omega, b)\mathrm{d}b = \frac{2}{\pi}Z_1^2\alpha\left(\frac{c}{v}\right)^2\left[\xi K_0K_1 - \frac{v^2\xi^2}{2c^2}\left(K_1^2 - K_0^2\right)\right] \tag{3.11}$$

where $\xi = \omega R/\gamma v$

The photon energy spectrum depends on the time the target particle spends in the contracted electromagnetic fiel, i.e. on the minimum distance between the target and the charge and on the projectile velocity; the minimum photon wavelength is the width of the contracted field at the target. and the maximum photon energy is given by:

$$\omega^{\max} = \frac{\hbar}{\Delta t} \approx \frac{\gamma\hbar v}{b} \tag{3.12}$$

where γ is the Lorentz factor of the particle. For ultraperipheral collisions where $b_{min} = R_A + R_B$, the maximum photon energy is $\approx \frac{\gamma\hbar v}{R_A+R_B}$

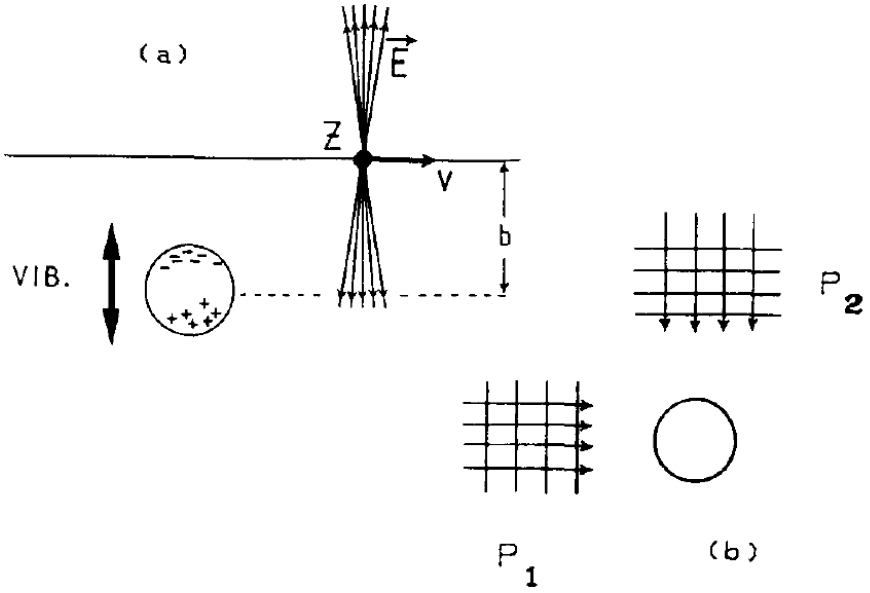

FIGURE 3.3: (a)A relativistic charged projectile incident on a target with impact parameter larger than the radii sum. (b) Two pulses of plane wave of light which produce the same effect on the target as the electromagnetic field created by the projectile's motion. [8]

3.2 Exclusive photonuclear vector meson production

Exclusive photonuclear vector meson production in relativistic heavy-ion are interactions of the type:

$$A + A \rightarrow A + A + V \tag{3.13}$$

It is the dominant coherent interaction leading to the production of a hadronic final state. The nuclei usually remain intact, and as it is a photonuclear interaction the vector meson is produced when a photon from the cloud of one of the nuclei interacts with the other nucleus. Using a change of variable from ω to y in 3.1 and differentiating respect to y, is possible to calculate the total vector meson cross section in p+p or A+A interactions.

$$\frac{\mathrm{d}\sigma(A + A \rightarrow A + A + V)}{\mathrm{d}y} = n\left(\omega\right)\sigma_{\gamma A \rightarrow VA}\left(\omega\right) \tag{3.14}$$

$$W_{\gamma N} = \sqrt{4\omega E_N} \tag{3.15}$$

$$W_{\gamma N} \approx 62GeV. \tag{3.16}$$

where $\omega = (M_v c^2/2)\exp\{y\}$, M_v is the vector meson mass. The Eq. 3.14 is a direct measure of the vector meson photoproduction cross section if the flux (ω) is known.

The production of light vector mesons at high energies can be described by the Meson Dominance Model(VMD); a photon radiated by the emitter nucleus fluctuates into a $q\bar{q}$ pair, is scattered elastically by the target nucleus and

emerges as vector meson. The cross section for the vector meson production depends on how the $q\bar{q}$ pair is coupled to the nucleus. The coupling is determined mainly by the transverse momentum; the cross section is bigger at low transverse momentum ($p_t < h/2\pi R_a$)[20]. The photon has quantum numbers $J^{PC} = 1^{--}$, so it mostly fluctuate into a vector meson. The uncertainty principle determine the lifetime of the fluctuation:

$$\Delta t \approx \frac{\hbar}{\sqrt{M_V^2 c^4 + Q^2 c^2}} \approx \frac{\hbar}{M_V c^2} \tag{3.17}$$

where Q is the photon virtuality of the photon and M_v is the mass of the vector meson the photon fluctuate in. According to VMD, the photon wave function can be written as[46]:

$$|\gamma\rangle = C_{\text{pure}} \left|\gamma_{\text{pure}}\right\rangle + C_{\rho^0}\left|\rho^0\right\rangle + C_\omega|\omega\rangle + C_\phi|\phi\rangle + C_{J/\psi}|J/\psi\rangle + \cdots + C_{q\bar{q}}|q\bar{q}\rangle \tag{3.18}$$

where $C_pure \approx 1$, and the amplitude C_V ($V = \rho^0, \omega, \phi....$), for the photon to fluctuate into vector meson V is:

$$C_V = \frac{\sqrt{4\pi\alpha}}{f_V} \tag{3.19}$$

where f_V is the photon vector meson coupling, and α is the electromagnetic coupling constant. The ρ^0 gives the dominant contribution to the photon hadronic structure, and its photoproduction has been measured at STAR[21] and ALICE[13] experiments. The scattering amplitude for the process $\gamma + A \to V + A$ can be written as:

$$A_{\gamma+A\to V+A}(s,t) = C_V A_{V+A\to V+A}(s,t) \tag{3.20}$$

The cross section is then:

$$\frac{d\sigma(\gamma + A \to V + A)}{dt} = C_V^2 \frac{d\sigma(V + A \to V + A)}{dt} \tag{3.21}$$

where t is the momentum transfer from the target nucleus squared and $d\sigma/dt = |A^2|$

The hadronic form factor $F(t)$ determine the momentum transfer:

$$\frac{\mathrm{d}\sigma}{\mathrm{d}t} = \left.\frac{\mathrm{d}\sigma}{\mathrm{d}t}\right|_{t=0} |F(t)|^2 \tag{3.22}$$

The form factor reflects the size and shape of the target. And if the spatial distribution is known is possible calculate it. The forward scattering amplitude, $d\sigma/dt(t = 0)$, contains the dynamical information, and is related to the total vector meson cross section $\sigma_{tot}(VA)$, through the optical theorem:

$$\left.\frac{\mathrm{d}\sigma}{\mathrm{d}t}\right|_{t=0} = C_V^2 \frac{\sigma_{tot}^2(VA)}{16\pi\hbar^2}\left(1 + \eta^2\right) \tag{3.23}$$

where η is the ratio of the real to the imaginary part of the scattering amplitude.

The forward scattering amplitude for heavy vector mesons has been calculated using the two gluon exchange in QCD. to leading order the result was:

$$\left.\frac{\mathrm{d}\sigma(\gamma p \to Vp)}{\mathrm{d}t}\right|_{t=0} = \frac{\alpha_s^2 \hbar^2 \Gamma_{ee}}{3\alpha M_V^5 c^6} 16\pi^2 \left[xg\left(x, M_v^2/4\right)\right]^2 \tag{3.24}$$

x is the fraction of the proton or nucleon momentum carried by the gluons and the gluon distribution,$g(x, Q^2)$, is evaluated at a momentum transfer $Q^2 = (M_V/2)^2$

The dependence of $d\sigma/dt$ on$[g(x)]^2$ makes exclusive vector meson production a very sensitive probe of the proton and nuclear gluon distributions.

3.3 Ultraperipheral collisions at STAR-RHIC

The Relativistic Heavy-Ion Collider (RHIC) at Brookhaven National Laboratory began operating in the year 2000. It consists of two independent 3.8 kilometer rings where heavy ions or protons circulate in opposite directions, it has six interaction points, in two of them are the largest experiments of this accelerator, the STAR experiment and the PHOENIX experiment. Particle production in ultra-peripheral collisions has been studied by both experiments. Some of the STAR results will be discussed in the following two subsections.

The STAR detector specializes in tracking the thousands of particles produced by each ion collision at RHIC. Weighing 1,200 tons and as large as a house, STAR is a massive detector. The primary physics task of STAR is to study the formation and characteristics of the quark-gluon plasma (QGP),

3.3.1 Coherent Photoproduction of $\rho^0(770)$

The first results on particle production in ultra-peripheral collisions at RHIC were studies of coherent production of ρ^0 mesons in Au+Au interaction by the STAR collaboration. [18] There are several models that describe the production of $\rho^0(770)$ mesons in ultraperipheral collisions: The model of Klein and Nystrand (KN) [40] uses the Vector Dominance Model (VDM) for the virtual photon and a classical mechanical approach for the scattering on the target nucleus, based on data from $\gamma p \to \rho^0 p$ experiments. The Frankfurt, Strikman, and Zhalov (FSZ) model [42] employs a generalized VDM to describe the virtual photon and a QCD Gribov-Glauber approach for the scattering. The model of Goncalves and Machado (GM) [29] takes into account nuclear effects and parton saturation phenomena by using a QCD color dipole approach.

In STAR, the coherent photoproduction of ρ^0 has been measured at $\sqrt{S_{NN}} = 62.4$[15], $\sqrt{S_{NN}} = 130$[18] and $\sqrt{S_{NN}} = 200$[16].

As in ALICE (see next chapter), the charged particles are reconstructed in a cylindrical TPC. The TPC in STAR is surrounded by 240 Central Trigger Barrel scintillator salts. There are are two Zero Degree Calorimeters located at $\pm 18m$ of the interaction point. Three different triggers were used for UPC collisions; a

Data sample	M_{ρ^0} (MeV/c^2)	Γ_{ρ^0} (MeV/c^2)	$\lvert B/A \rvert$
62.4 GeV	764 ± 9	140 ± 13	0.88 ± 0.009
130 GeV	777 ± 7	139 ± 13	0.81 ± 0.08
200 GeV	775 ± 3	162 ± 7	0.89 ± 0.08

TABLE 3.1: Invariant mass, width and $\lvert B/A \rvert$ ratio of three different data samples from STAR

topology trigger and two minimum bias triggers, For the topology trigger the CTB was divided in four azimuthal quadrants. A coincidence between left– and right–side quadrants was required. The first minimum bias (A) required a coincidence signal in both ZDCs. The second minimum bias(B) trigger further requiered a charged particle signal in the CTB.

The first minimum bias (A) trigger was used for the study at the three energies, the topological trigger was used at $\sqrt{S_{NN}} = 130$ and $\sqrt{S_{NN}} = 200$, and the second minimum bias trigger(B) was used at $\sqrt{S_{NN}} = 62.4$.

For the analysis of the three data samples events with exactly two oppositely charged tracks, from a common vertex, were selected. A ρ^0 event from photoproduction should have exactly two tracks in the TPC, but additional tracks may come from overlapping interactions, including beam-gas interactions. Events with at least one neutron (xn, xn), exactly one neutron (1n, 1n), or no neutrons (0n, 0n) in each ZDC, and events with at least one neutron in exactly one ZDC (xn, 0n), were selected using the energy deposit in the ZDCs. The latter two can only occur with the topology trigger. The selected events were required to have $pT < 150 MeV/c$.

The invariant mass distribution for ρ^0 candidates, from the minimum bias trigger and the topological trigger, for the sample at $\sqrt{S_{NN}} = 200$ is shown in figure 3.4. The distribution is fitted with a formula due to Soding, where a continuum amplitude, B, is added to a Breit-Wigner resonance [47]:

$$\frac{d\sigma}{dM_{\pi\pi}} = \left| A \frac{\sqrt{M_{\pi\pi} M_{\rho^0} \Gamma_{\rho^0}}}{M^2_{\pi\pi} - M^2_{\rho^0} + i M_{\rho^0} \Gamma_{\rho^0}} + B \right|^2 + f_p \tag{3.25}$$

Here, A is the amplitude of the Breit–Wigner function, B is the amplitude of the direct non–resonant $\pi^+\pi^-$ production,M_{ρ^0} is the ρ^0 mass, f_p is a second order polynomial used to describe the background, and the mass dependent width is given by

$$\begin{aligned} \Gamma_{\rho^0} =& \Gamma_0 \cdot \left(M_{\rho^0} / M_{\pi^+\pi^-} \right) \\ & \times \left[\left(M^2_{\pi^+\pi^-} - 4m^2_\pi \right) / \left(M^2_{\rho^0} - 4m^2_\pi \right) \right]^{3/2} \end{aligned} \tag{3.26}$$

The values obtained from the fit for the mass, the width and the $\lvert B/A \rvert$ ratio, for the three data samples are shown in table 3.1.

The calculated cross sections for the three data samples extrapolated to the full 4π acceptance in y, is shown in table3.2. In figure 3.5 the calculated differential cross section at $\sqrt{S_{NN}} = 200$ is compared with the theoretical models.

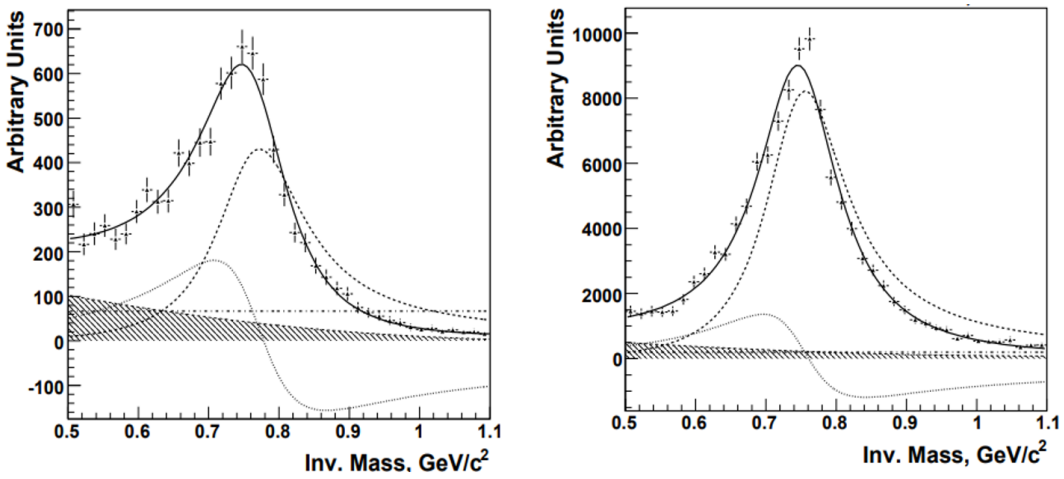

FIGURE 3.4: The invariant mass distribution for the coherently produced ρ^0 candidates from the minimum bias sample(left). The invariant mass distribution for the coherently produced ρ^0 candidates obtained from the topology sample (right) [16]

Cross section	$\sqrt{s_{NN}} = 62.4$GeV	$\sqrt{s_{NN}} = 130$GeV	$\sqrt{s_{NN}} = 200$GeV
$\sigma^{\rho^0}_{\mathrm{XnXn}}$(mb)	$10.5 \pm 1.5 \pm 1.6$	$28.3 \pm 2.0 \pm 6.3$	$31.9 \pm 1.5 \pm 4.5$
$\sigma^{\rho^0}_{\mathrm{0nXn}}$(mb)	$31.8 \pm 5.2 \pm 3.9$	$95 \pm 60 \pm 25$	$105 \pm 5 \pm 15$
$\sigma^{\rho^0}_{\mathrm{0n0n}}$(mb)	$78 \pm 14 \pm 13$	$370 \pm 170 \pm 80$	$391 \pm 18 \pm 55$
$\sigma^{\rho^0}_{\mathrm{total}}$ (mb)	$120 \pm 15 \pm 22$	$460 \pm 220 \pm 110$	$530 \pm 19 \pm 57$

TABLE 3.2: Total cross section extrapolated to the full rapidity range for coherent ρ^0 production at $\sqrt{S_{NN}} = 62.4$, $\sqrt{S_{NN}} = 130$ and $\sqrt{S_{NN}} = 200$

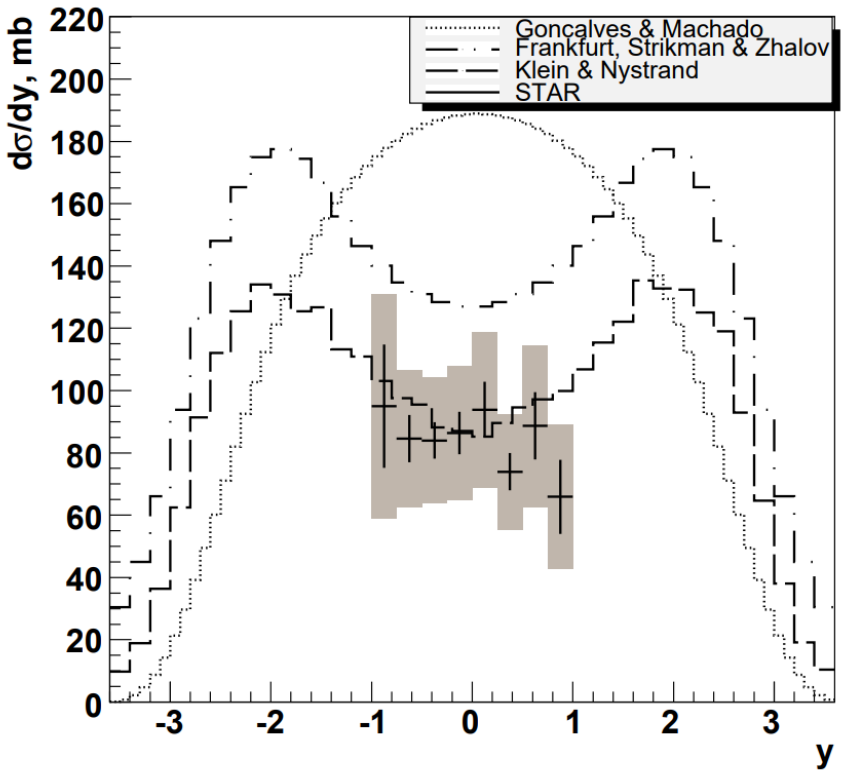

FIGURE 3.5: Comparison of theoretical predictions to the measured differential cross-section for coherent ρ^0 production [16]

3.3.2 $\pi^+\pi^-\pi^+\pi^-$ photoproduction

Coherent $\pi^+\pi^-\pi^+\pi^-$ production in ultraperipheral collisions accompanied by mutual nuclear dissociation of the beam ions was measured in Au-Au collisions at $\sqrt{S_{NN}} = 200$ [19] using the minimum bias data, where the minimum bias trigger is of type B. In the offline analysis two- and four-tracks data sets are selected. Four-tracks events are required to have exactly four tracks with zero net charge in the TPC that form a common (primary) vertex. The transverse momentum distribution of the $\pi^+\pi^-\pi^+\pi^-$ combinations is shown in 3.6, it exhibits an enhancement at low pT which is a characteristic of coherent production.

The invariant mass distribution, figure 3.7, was fitted in the range from 1 to 2.6GeV/c^2 with a relativistic S-wave Breit-Wigner modified by the phenomenological Ross-Stodolsky factor [44]:

$$f_{4\pi}(m) = A \cdot \left(\frac{m_0}{m}\right)^n \cdot \frac{m_0^2\Gamma_0^2}{\left(m_0^2 - m^2\right)^2 + m_0^2\Gamma_0^2} + f_{\mathrm{BG}}(m) \tag{3.27}$$

Here m is the$\pi^+\pi^-\pi^+\pi^-$ invariant mass. The resonance mass m_0, the width Γ_0, and the exponent n are left as free parameters. The non-interfering background f_{BG} was parameterized by a second order polynomial which was extracted from the invariant mass distribution of +2 or 2 charged four-prongs. Taking into account the experimental acceptance, the fit yields a resonance

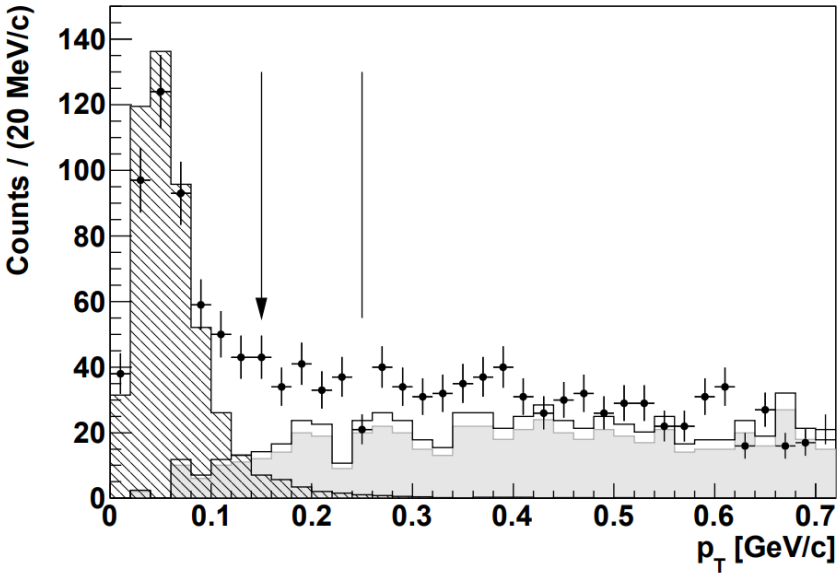

FIGURE 3.6: Distribution of the $\pi^+\pi^-\pi^+\pi^-$ transverse momentum [19]

mass of $1540 \pm 40 MeV/c^2$ and a width of $570 \pm 60 MeV/c^2$ in agreement with the photoproduction data for the $\rho(1700)$. The Ross-Stodolsky exponent has a value of $n = 2.4 \pm 0.7$. The mass and the width depend strongly on the value of n.

For the acceptance and efficiency corrections was estimated using a Monte Carlo Monte Carlo event generator based on the KN model [39]. A model, where an excited ρ^0 meson decays into ρ^0 and f0(600), each in turn decaying into $\pi^+\pi^-$

$$\rho' \to \rho^0(770) f_0(600) \to \left[\pi^+\pi^-\right]_{P-\text{ wave}} \left[\pi^+\pi^-\right]_{S-\text{ wave}} \tag{3.28}$$

This decay model is motivated by the fact that the invariant mass spectrum of the unlike-sign two-pion subsystems in the four-prong sample shows an enhancement around the $\rho^0 mass$, figure 3.8 show the invariant mass spectrum of the lightest pair $\pi^+\pi^-$ with invariant mass spectrum of the pair recoiling against it, so the model use for the MC reproduces the data well. Using the acceptance yield corrected for $\pi^+\pi^-\pi^+\pi^-$ the ratio of $\rho^0(1700)$ and ρ^0 coherent production cross sections is measured to be $13.4 \pm 0.8 stat. \pm 4.4 syst.\%$.

3.4 Ultraperipheral collisions at ALICE-LHC

3.4.1 Coherent ρ^0 photoproduction in Pb–Pb UPC

ALICE has published results on coherent ρ^0 photoproduction in Pb–Pb UPC [17] showing good agreement with STARLIGHT(KN Model)[40, 39] predictions.

Data collected during the 2010 Pb–Pb run of the LHC at an energy of $\sqrt{S_{NN}} = 2.76 TeV$ were used for this analysis. Two different triggers were used. For the

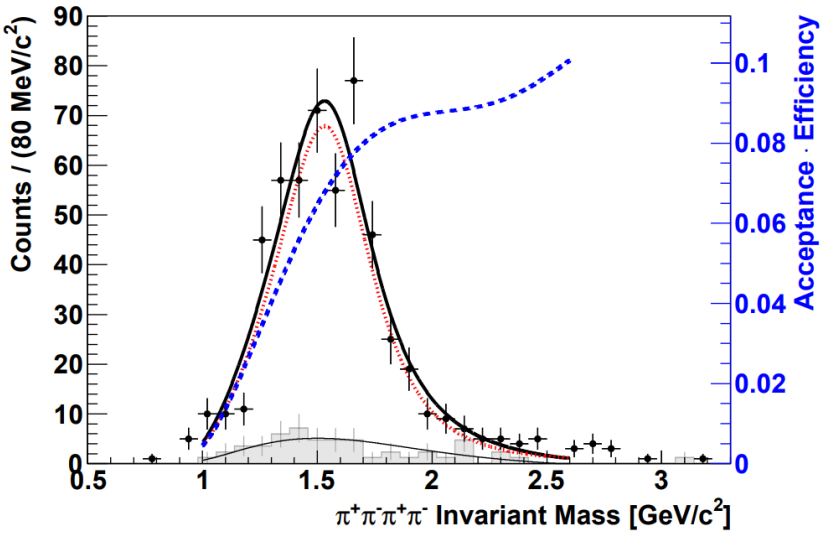

FIGURE 3.7:) Invariant mass distribution of coherently produced $\pi^+\pi^-\pi^+\pi^-$ [19]

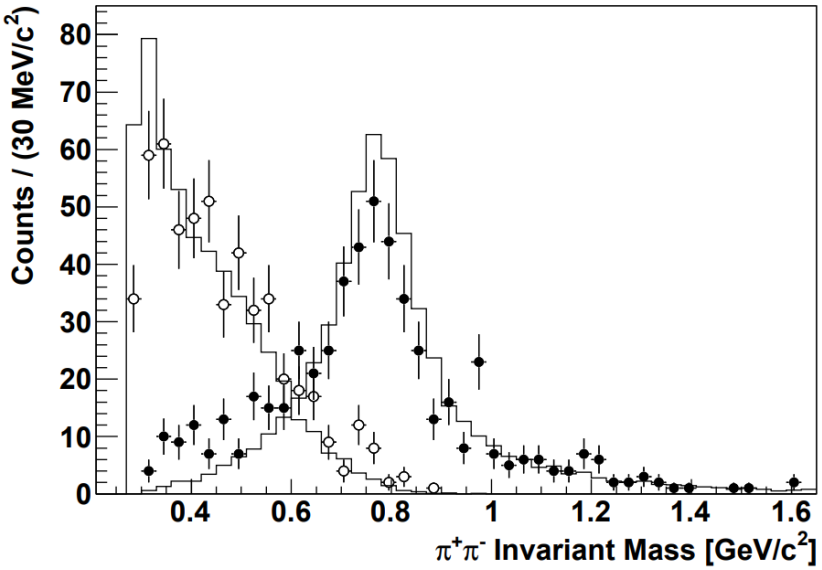

FIGURE 3.8: Invariant Mass distribution of two-pion subsystems; The open circles show the measured invariant mass spectrum of the lightest $\pi^+\pi^-$ pair in the event with the bars indicating the statistical errors. The filled circles represent the invariant mass distribution of $\pi^+\pi^-$ the that is recoiling against the lightest pair [19]

first runs, the trigger requirement was at least two hits in the TOF detector, due the luminosity was low. When the luminosity was increased the trigger required additionally at least two hits in the outer layer of the SPD, and no activity in any of the VZERO arrays. The offline requiremnts for the events were:

- A primary vertex in $\pm 10cm$ in the beam direction
- Events with exactly two tracks reconstructed in ITS and TPC
- VZERO detectors required to be empty
- The energy loss in the TPC has to be consistent with that for pions within 4 standard deviations from the Bethe-Bloch expectations.
- Events with low transverse momentum (pT$< 150MeV/c^2$ and $|y| < 0.5$)
- Opposite charge tracks.

The two-pion transverse momentum distribution around the ρ^0 mass is shown in figure 3.9, The distribution is compared with the corresponding distributions from STARLIGHT [16, 23] events for coherent and incoherent ρ^0 production, processed through the detector response simulation based on GEANT 3. The coherent peak is shifted to slightly lower pT in data than that predicted by STARLIGHT. The invariant mass distribution of the ρ^0 candidates, corrected for acceptance and efficiency and normalized by the luminosity, is shown in figure 3.10 the fit to the spectrum was done using Soding formula given Eq 3.25 and a a Ross-Stodolsky function [44]:

$$\frac{\mathrm{d}\sigma}{\mathrm{d}M_{\pi\pi}} = f \left| \frac{\sqrt{M_{\pi\pi} M_{\rho^0} \Gamma\left(M_{\pi\pi}\right)}}{M_{\pi\pi}^2 - M_{\rho^0}^2 + i M_{\rho^0} \Gamma\left(M_{\pi\pi}\right)} \right|^2 \left(\frac{M_{\rho^0}}{M_{\pi\pi}} \right)^k \tag{3.29}$$

where the mass dependent width is given by:

$$\Gamma\left(M_{\pi\pi}\right) = \Gamma_{\rho^0} \left[\frac{M_{\pi\pi}^2 - 4m_\pi^2}{M_{\rho^0}^2 - 4m_\pi^2} \right]^{\frac{3}{2}} \tag{3.30}$$

The fit to the Soding formula gave the following values: $M_{\rho^0} = 761.6 \pm 2.3(\text{ stat. })^{+6.1}_{-3.0}(\text{ syst.})\text{MeV}/c^2$ and $\Gamma_{\rho^0} = 150.2 \pm 5.5(\text{ stat. })^{+12.0}_{-5.0}$ (syst.) MeV/c^2, in agreement with the values reported by the PDG []. The ratio of the non-resonant and resonant amplitudes is found to be $|B/A| = 0.50 \pm 0.04(\text{ stat. })^{+0.10}_{-0.04}($ syst. $)$

The fit to the Ross-Stodolsky function gave the following values: $M_{\rho^0} = 769.2 \pm 2.8(\text{ stat. })^{+8.0}_{-5.2}(syst.)\text{MeV}/c^2, \Gamma_{\rho^0} = 156.9 \pm 6.1(\text{ stat. })^{+17.3}_{-5.9}(syst.)\text{MeV}/c^2$, consistent with the PDG values. The deviation from a pure Breit-Wigner shape is given by the parameter k, which was found to be $k = 4.7 \pm 0.2(\text{ stat. })^{+0.8}_{-0.6}(syst.)$. Comparing the value of k obtained here with the one obtained in proton collisions from ZEUS [] and H1 [] at HERA. Z(which was $k = 6.84 \pm 1$ averaged

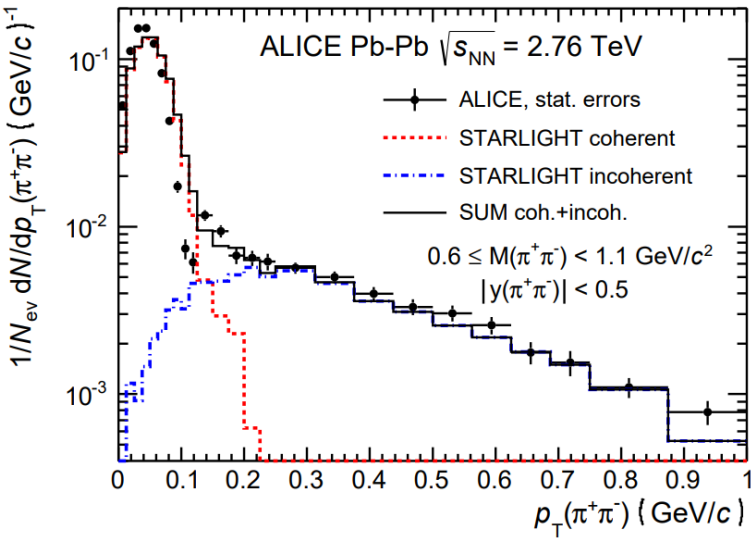

FIGURE 3.9: Transverse momentum distributions for$\pi^+\pi^-$ pairs[17].

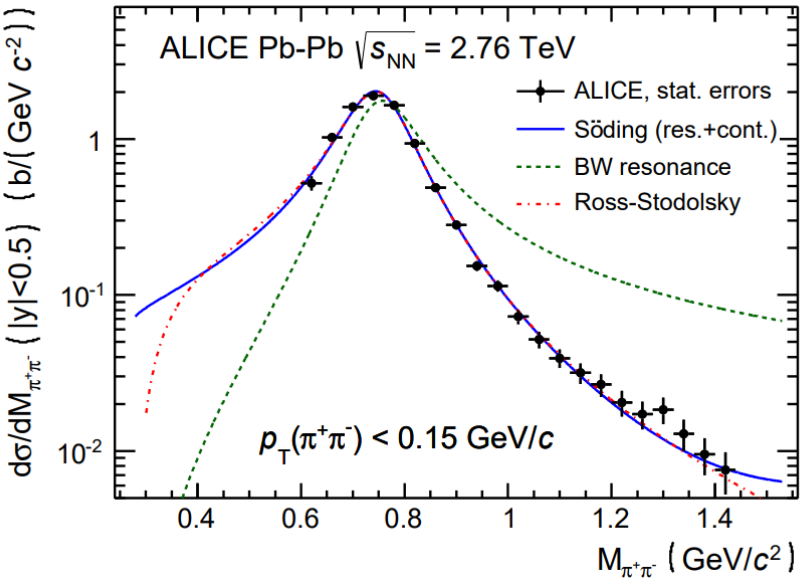

FIGURE 3.10: Invariant mass distribution for $\pi^+\pi^-$ pairs corrected for acceptance and efficiency [17]

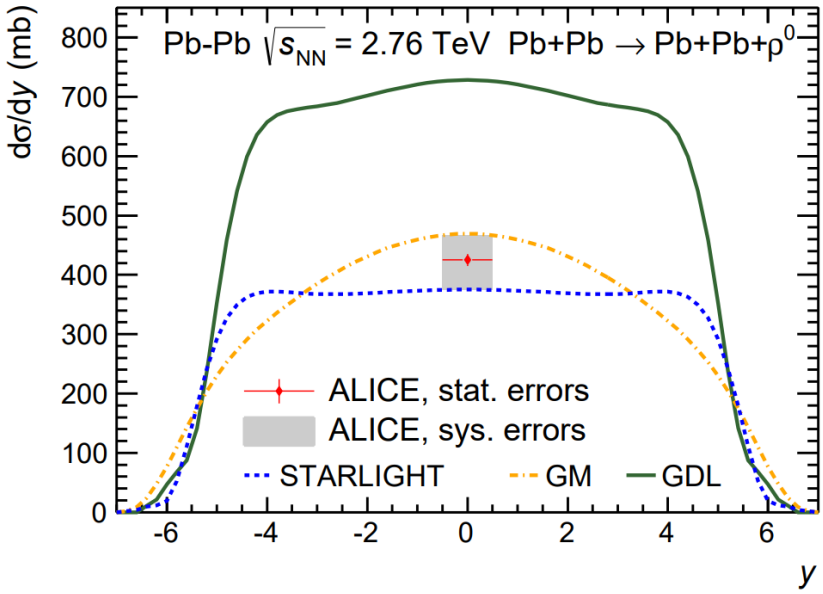

FIGURE 3.11: Cross section for coherent photoproduction of ρ^0 , $d\sigma/dy$, in ultraperipheral collisions for the three models compared with the ALICE result[17]

over all momentum transfers), we can notice that the invariant mass distribution for Pb-targets deviates less from a pure Breit-Wigner resonance than for p-targets , as was also found using the Soding formula.

The calculated cross section for the sample taken only with the TOF trigger is $\frac{d\sigma}{dy} = 466 \pm 25mb$, and for the sample using the SPD+TOF+VZERO trigger is $\frac{d\sigma}{dy} = 414^{+14}_{-16}mb$, the final cross section is obtained as the weighted mean of the cross sections of the two samples, and is $\frac{d\sigma}{dy} = 425 \pm 10(stat.)^{+42}_{-50}(syst.)mb$. The coherent ρ^0 photoproduction cross section, is shown and compared with model predictions in figure 3.11. The measured cross section is in agreement with STARLIGHT[40] and the calculation by Goncalves and Machado (GM)[30]. The GDL (Glauber-Donnachie-Landshoff) prediction [41]is about a factor of 2 higher than data. The calculation by GM is based on the Color Dipole model, while STARLIGHT and GDL use the photon-proton cross section $\sigma(\gamma + p \rightarrow \rho^0 + p$ constrained from data as input.

Chapter 4

The ALICE Experiment

The ALICE(A Large Ion Collider) experiment [7] is a multipurpose heavy ion experiment located in the large hadron collider(LHC) at CERN. It was designed to address the physics of strongly interacting matter and the quark-gluon plasma at extreme values of energy density and temperature in nucleus-nucleus collisions. The QCD (quantum chromodynamics) predicts the existence of a state of deconfined quarks and gluons at energy densities above $1GeV/fm^3$, such energy densities can be reached right after heavy ion collisions, although just for a small amount amount of time in a small space region right after the collision. Besides Pb-Pb collisions, p-p, p-Pb and Xe-Xe collisions are studied at ALICE.

The ALICE detector was built by a collaboration conformed by more than 1000 physicists and engineers from 105 institutes of 30 countries, including Mexico. The detector have an approximate weights of 10 000 t, and a volume of $6656m^3$

In ALICE as well as in other particle collision experiments two types of detectors are used; Calorimeters and Trackers. The Calorimeters are designed to measure the energy of particles when they go through it; when a particle passes through a calorimeter a photon shower is generated, the photons are collected and used to measure the energy of the initial particle. The calorimeters are typically made of a highly dense material in order to trap the particle and, therefore, its whole energy were deposited in the calorimeter. The Trackers are used to determine the trajectories of the particles that pass through it, and are are designed to barely interact with such particles, so the trajectories are not affected.

ALICE is conformed by central barrel detectors(which measures hadrons, electrons, and photons), forward detectors and a muon spectrometer. The ALICE schematic layout is shown in figure 4.1. The ALICE central barrel detectors(from inner to outer: Inner Tracking System (ITS), Time Projection Chamber (TPC), Transition Radiation Detector (TRD), Time Of Flight (TOF), Photon Spectrometer (PHOS), Electromagnetic Calorimeter (EMCal), and High Momentum Particle Identification Detector (HMPID)), which enclose the interaction point, are embedded in a solenoid with magnetic field $B = 0.5T$. Considering the axis z in the same direction of the beam pipe, most of the detectors cover the full azimuth angle, except HMPID, PHOS, and EMCal. The polar angle coverage varies between 45° to 135°. The ITS and the TPC are used for charged-particle tracking and identification. The identification is done via measurement of ionization energy loss (dE/dx). TRD detector is used for

charged-particle tracking and for electron identification via transition radiation and dE/dx.The TOF detector is used for particle identification at intermediate momenta. PHOS,EMCal and HMPID are also used for charged-hadron identification.

The forward detectors are located at small angles in front and behind the interaction point; the Photon Multiplicity Detector (PMD), the silicon Forward Multiplicity Detector (FMD), The quartz Cherenkov detector T0, The plastic scintillator detector V0 and the Zero Degree Calorimeter (ZDC). The principal functions of these detectors are the event characterization and triggering.

In 2015 the detector AD(ALICE Diffractive), made by a Mexican Collaboration, was installed, and as its name implies, it is used mainly for diffractive process studies.

The MUON spectrometer and five tracking stations with two pad chambers each (Muon Chambers, MCH) are used to measure quarkonium and light vector meson production.

ACORDE was a scitillator plastic array located on top of the solenoid and used to study cosmic rays and for calibration of the other detectors. It is no longer part of the ALICE detector, it was uninstalled during 2019.

Due to the geometry and position of detectors, the acceptance in η and ϕ and the effective detection area from each detector are different. Not all the detectors can measure the same particles and physics events.

In table 4.1 a summary of the detectors is presented, acceptance in η is shown for every detector, acceptance in ϕ is shown for detectors that not cover the 360 degrees. The approximate distance from detectors to the interaction point is indicated, for the barrel detectors the inner and outer radius are given. Finally the area covered by active detector elements and the number of independent electronic readout channels is shown .

Below, a brief description of the most relevant detectors for this study is presented. For a more detailed description see reference 4.1.

4.1 Inner Tracking System (ITS)

The Inner tracking System (ITS) [24] is part of the central barrel detectors and is the one with the the smallest radial distance about the beam axis, it surrounds the beam pipe an also provides mechanical support to it. The main tasks of ITS are:

- Primary vertex reconstruction (with a resolution better than 100μm)
- Secondary vertex reconstruction from hyperons and D and B mesons decays
- Tracking and identification of low momentum particles (P<200 MeV/c)
- Improve the momentum and angle resolution for particles reconstructed by TPC.
- Reconstruct particles that pass through dead regions of the TPC

Detectors		Acceptance η and ϕ	Distance	Area	Channels
ITS	SPD (layer 1 y 2)	$\pm 2, \pm 1.4$	0.039-0.076	0.21	9.8 M
	SDD (layer 2 y 4)	$\pm 0.9, \pm 0.9$	0.15-0.239	1.31	2.6M
	SSD (layer 5 y 6)	$\pm$ 0.97,$\pm$0.97	0.380-0.430	5.0	2.6M
TPC		$\pm$ 0.9	0.848-2.466	32.5	557568
TRD		$\pm$0.84	2.9-3.68	716	1.2M
TOF		$\pm$0.9	3.78	141	157248
HMPID		$\pm 0.6, 1.2^o < \phi < 58.8^o$	5.0	11	161280
PHOS		$\pm 0.12, 220^o < \phi < 320$	4.6	8.6	17920
EMCal		$\pm 0.7, 80^o < \phi < 187^o$	4.36	44	17920
ACORDE		$\pm 1.3, -60^o \vert \phi < 60^o$	8.5	43	120
ZDC	ZN	$\pm$8.8	$\pm$116	2x0.0049	10
	ZP	$6.5 < \vert\eta\vert < 7.5$ $-9.7^o < \phi < 9.7^o$	$\pm$116	2x0.027	10
	ZEM	$4.8 < \vert\eta\vert < 5.7$ $-16^o < \phi < 16^o$ $164^o < \phi < 196^o$	7.25	2x0.0049	2
PMD		2.3<η<3.7	3.64	2.59	2221184
FMD	disc 1	3.62<η<5.03	3.2	0.266	51200
	disc 2	1.7<η<3.68	inner:0.834 outer=0.752	0.266	51200
	disc 3	-3.4<η<-1.7	inner -0.628 outer:-0.752	0.266	51200
V0A		$2.8 < \eta < 5.1$	3.4	0.548	32
V0C		$-1.7 < \eta < -3.7$	-0,897	0.315	32
TOA		$4.61 < \eta < 4.92$	3.75	0.0038	32
T0C		$-3.28 < \eta < -2.97$	-0.727	0.0038	12

TABLE 4.1: ALICE detectors summary[7]

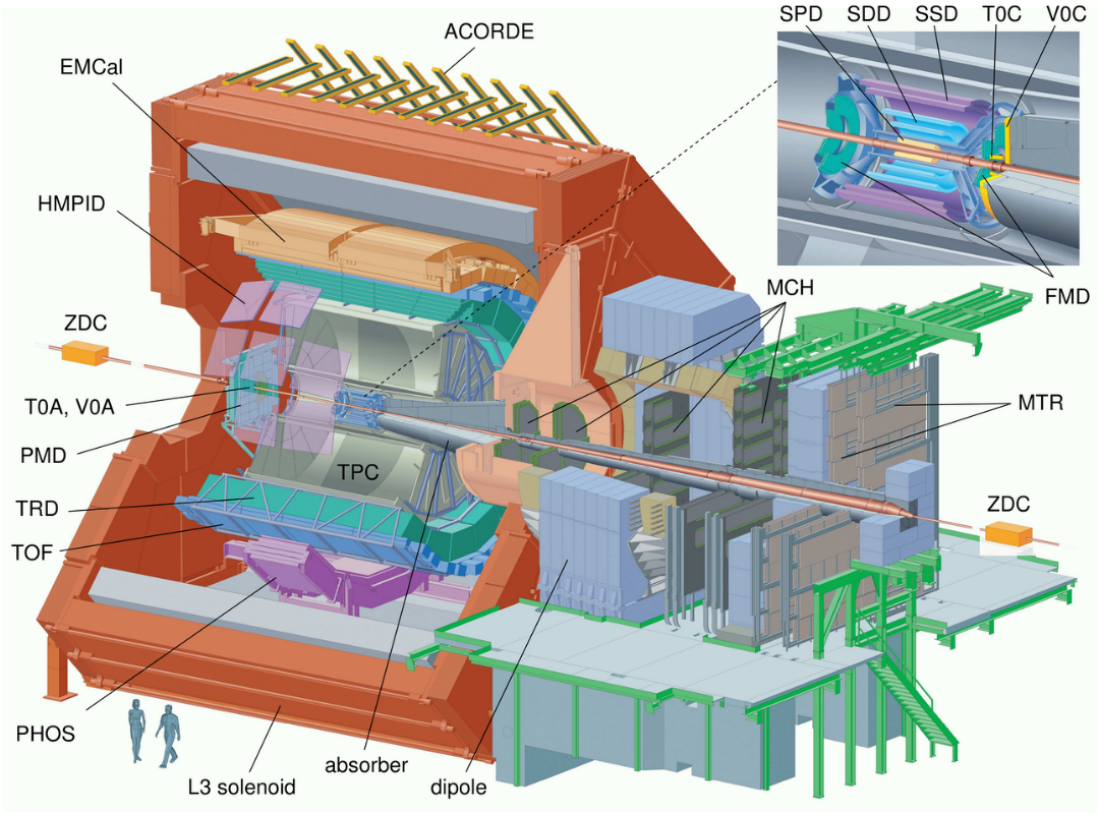

FIGURE 4.1: Alice experiment[7]

The ITS is used in practically all the physical studies for the reasons listed above.

Six cylindrical layers of silicon detectors conform the ITS (see figure 4.2), the layers are coaxial with the beam pipe an are located at a radial distance between 4 and 43cm, and have a lenght of 98cm. The rapidity range for all the layer is $\eta < 0.9$, except for the first layer , which has a coverage $\eta < 1.98$.

A particle density of up to 50 particles$/cm^2$ is expected in heavy ion collisions at the LHC, because of that and in order to achieve the required impact parameter resolution, the two innermost layers of the ITS are conformed by Silicon Pixel Detectors(SPD), the following two by Silicon Drift Detectors(SDD), and the two outer layers by double-sided Silicon micro-Strip Detectors(SSD). In these two last layers the desnsity is expected to be below 1 particle$/^2$. The 4 outer layers can be used for particle identification via dE/dx measurement in the non-relativistic $(1/\beta^2)$ region.

4.2 Time Projection Chamber (TPC)

A Time Projection Chamber is a particle detector that consists of a volume(usually a cylinder) filled with gas, with a layer of multi-wire proportional chambers (MWPC) in each end plate. The volume is divided in two equal parts by a central high-voltage electrode disc. An uniform electric field is set between the electrode and the end plates. A charged particle traversing the volume ionise the gas along its path, liberating electrons that drift towards the end plates of

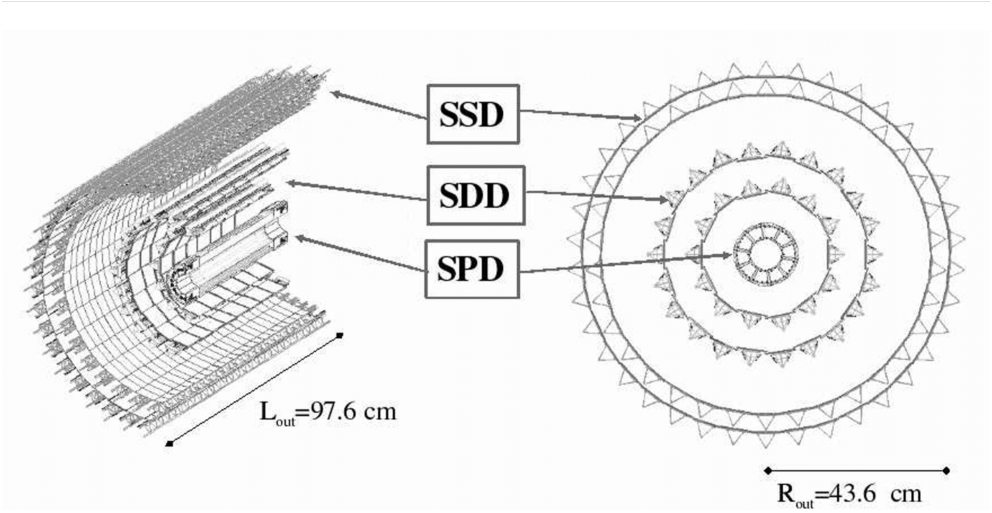

FIGURE 4.2: ITS layout[7]

the cylinder, so this way is possible obtain a 3-D reconstruction of the particle trajectory. To minimize electron diffusion and have a better trajectory reconstruction a magnetic field, parallel to the electric field, can be applied.

The TPC was invented by Dave Nygren at the Lawrence Berkeley Laboratory (LBL) in the late 1970s.

In ALICE, the TPC [26] is the main tracking detector of the central barrel and is used to provide, together with the other central barrel detectors, charged-particle momentum measurements with good two-track separation, particle identification, and vertex determination, In addition, data from the central barrel detectors are used to generate a fast online High-Level Trigger (HLT) for the selection of low cross section signals.

The shape of ALICE TPC is as the original TPC, a cylinder, with an inner and outer radius of 85cm and 250 cm, respectively, a lenght of 510cm. The volume is about $90m^3$, and is filled with a gas mixture: 85.7% Ne, 9.5% CO_2 and 4.8% N_2. Multi-wire proportional chambers with cathode pad readout are mounted into 18 trapezoidal sectors at each end plate. In figure 4.3 the ALICE TPC layout is shown. The TPC covers a pseudorapidity range of $|\eta| < 0.9$ and cover the full range in the azimuthal angle. It is designed to handle multiplicities up to $dN_ch/d\eta = 8000$, which is equivalent to 20,000 primary and secondary traces within the acceptance range of the TPC. This multiplicity value was estimated for Pb-Pb collisions. A wide range in transverse moment (Pt) is covered by the TPC, from 0.1GeV/c to 100GeV/c, with good momentum resolution.

4.3 V0

The V0 [6] detector measure particles produced in collisions whose trace forms a small angle with respect to the beam axis, it consists of 2 counter arrays of scintillating plastic, called V0A and V0C, which are located asymmetrically on

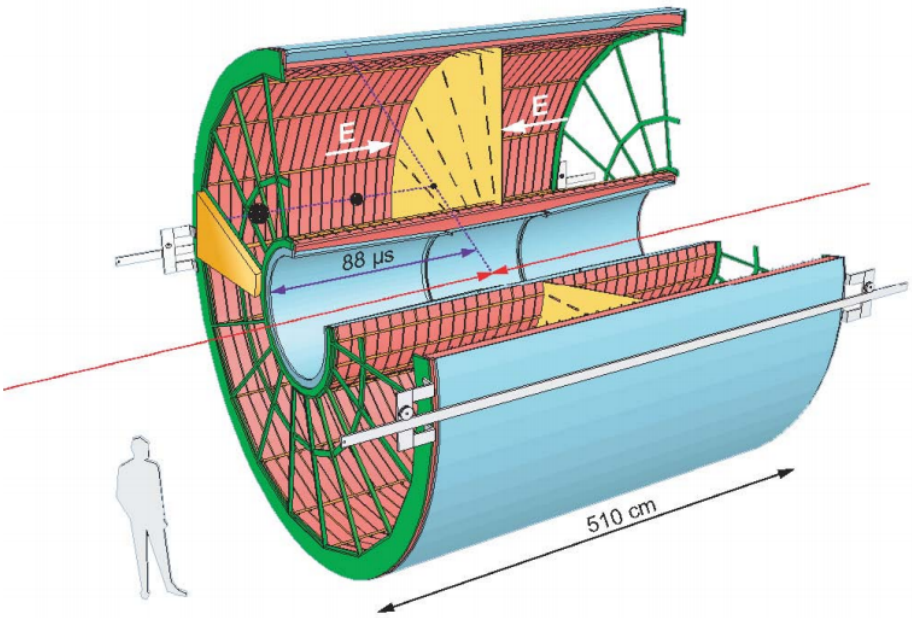

FIGURE 4.3: TPC[7]

both sides of the interaction point. The V0A detector is located 340cm from the interaction point(opposite to the muon spectrometer side), it has a pseudorapidity acceptance of 2.8 $<\eta<$5.1. While the V0C detector is located 90cm from the interaction point and has a pseudorapidity acceptance of 3.7 $<\eta<$1. Both V0A and V0C are segmented into 32 individual counters which are distributed in 4 rings (fig 4.4).

The counters consist of scintillating plastics with wavelenght shift(WLS) fibres embedded, as indicated in its the name the WLSfibres change the wavelenght of the photons produced from the interaction of a charged particle with the detector, these photons are collected transported to a photomultiplier. The time resolution of each counter in the order of 1ns. The V0 detector tasks are:

- Provide minimum bias trigger signals for center barrel detectors in p-p and Pb-Pb collisions
- Each of the 64 channels can measure the charge of the incident particles and the moment at their arrival
- Serve as an indicator of the centrality of the collision according to the multiplicity recorded in the event; there is a monotone dependence between the number of particles recorded in the V0 arrays and the number of primary particles emitted
- Measurement of luminosity in pp collisions with a good precision of about 10%
- Identify Beam-Gas background; Due to the vacuum generated inside the beam tube is not ideal, there are gas particles inside it with which the beam particles can interact and generate background-fake signals in the

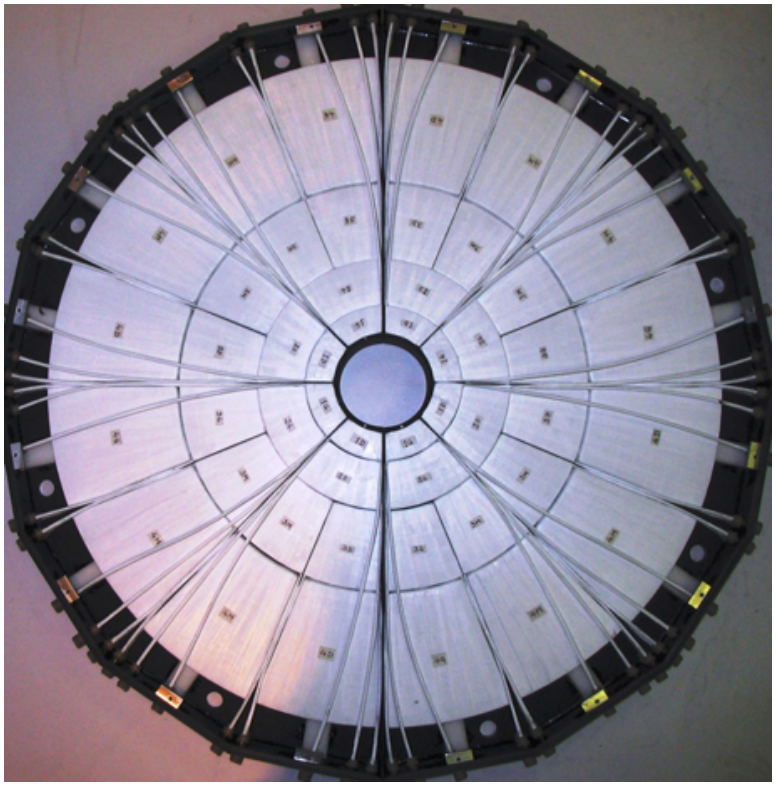

FIGURE 4.4: V0C detector[5]

detectors. The arrival time of the signal in the V0A and V0C modules is used in order to eliminate these noise signals

In the case of ultra–peripheral collisions the V0 detectors are used as veto detectors and are required to be empty in order to suppress avoid hadronic interactions.

4.4 ALICE diffractive (AD)

The AD detector (ALICE Diffractive) [3] is composed of 2 subdetectors called ADA and ADC, each one consists of 2 detector plates and each plate of four scintillation detector stations. It was integrated into the experiment and validated in 2012 as a diagnostic system. This is a detector dedicated to the study of hard and soft diffractive events in both p-p and Pb-Pb collisions. Due to its position, on the sides of the point where collisions occur, AD is an excellent detector, which allows ALICE to have adequate conditions to access the region of very low transverse moment of the particles produced, and with ALICE's good capacity to making identification, a wide range of diffractive physics can be explored within the LHC.

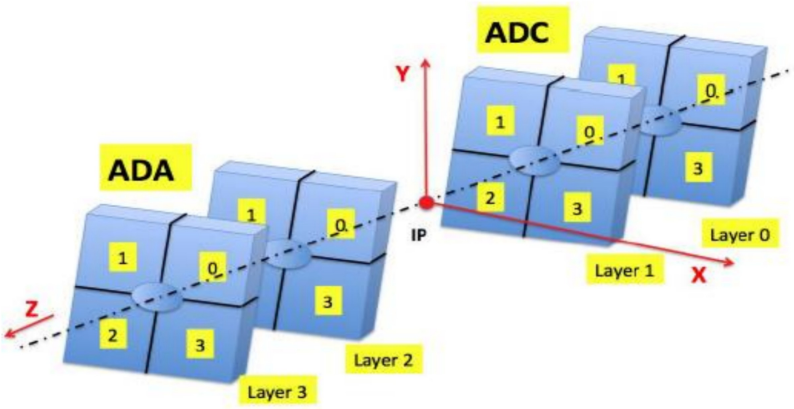

FIGURE 4.5: AD detector[3]

4.5 Time of Flight (TOF)

The TOF (Time Of Flight)[25] detector is made up of 1593 Multi-gap Resistive Plate Chambers(MRPCs) and divided into 18 sectors in the azimuthal component. Covers an area of $160m^2$, and is located at about 3.7m from the beam axis,the whole device is inscribed in a cylindrical shell with an internal radius of 370 cm and an external one of 399 cm. The TOF was primarily designed to achieve global time resolution around 100ps in order to identify kaons and pions above 2.5 GeV/c and protons above 4GeV/c in the pseudorapisity range $\eta < |0.9|$. The time measured by the TOF, in conjunction with the moment and the length of the trajectory measured by the TPC and the ITS, is used to calculate the mass of the particles. Charged-particle PID in the intermediate momentum range is provided by TOF. The TOF also provides a trigger for cosmic ray events and ultraperipheral collisions. A charged particle passing through a MRPC will ionize the detector material, a constant Electric field will accelerate the free electrons product of the ionization and will generate an avalanche effect, whichgenerates an observable signal in the electrodes. The MRPCs have an efficiency close to 100%. The TOF detector does not have any dead zones, the modules were designed in such a way so that any loss of sensitivity is avoided, on the z axis, the only dead section it is due to the presence of the support structure.

4.6 Trigger System

The trigger systems in ALICE can be configured to determine if an event should be collected or discarded, according to the physics that is being searched during the particles collisions. The triggers are generally formed by a set of detectors signals; according to such signals a decision is made on whether or not to collect the event. Clearly, this decision cannot take a long time since the collisions and particle production are almost continuous, the separation between beams is 25 nanoseconds.

4.6.1 Trigger Inputs

The ALICE trigger system can be divided in two main elements, the Central Trigger Processor(CTP) [2][48] and the High Level Trigger (HLT)[12], The CTP is a hardware trigger placed in the experiment cavern, while the HLT is mainly implemented as a software trigger. The CTP generates the trigger decision using the information from various detector signals; a "trigger input" is the signal from a triggering detector to the CTP and a "trigger signal" is the signal sent to the readout electronics of the detector by the CTP, the signal is sent by CTP to the detector Local Trigger Unit (LTU) which is the interface between the detector read-out and the CTP. The ALICE CTP generates three levels of hierarchical hardware triggers L0, L1 and L2:

- L0(Level 0): the trigger inputs arrive from the interaction to the CTP in approximately 1.2μs. The L0 can be labelled as L0a and L0b where the "a" stands for "after the CTP" and the "b" stands for "before the CTP". The ALICE trigger system has 24 L0 inputs. The L0 inputs activated for the 2018 in Pb-Pb collisions are shown in table 4.2.

- L1(Level 1): the L0 signal is too fast for some trigger inputs, therefore there is an additional L1 signal arriving 6.5μs after.The ALICE trigger system has 24 L1 inputs. The L1 inputs activated for the 2018 in Pb-Pb collisions are shown in table 4.3.

- Level 2 (L2) trigger is delivered after 105 μs from the interaction. The detector with the longest sensitive period in ALICE, the TPC, will register hits up to 88 µs from the time of an interaction. Therefore, the final level of the trigger (L2), cannot be given until after this period. The ALICE trigger system has 12 L2 inputs.

The trigger input detectors used for UPC in 2018 are TOF,SPD, V0 and AD.

4.6.2 Clusters and Classes

The set of readout triggers that participate in any given event are defined by a trigger cluster. Different trigger clusters can be configured in ALICE. A series of logical conditions(AND and OR) over the L0 inputs along with CTP vetoes, past future protection and region of interest make up a trigger class. A trigger class defines which detectors will work as trigger detectors for a specific type of event and, as mentioned before, The trigger cluster define which detectors should be used as readout detectors.

The name of a trigger class is a series of five elements that give information about the purpose and characteristics of the class:

1. descriptor: describe the trigger inputs

2. bunch crossing mask: B(means that there are beams from both sides), A(beam from A side), C(beam from C side), E(empty)

3. Past future protection scheme

Input ID	Input Name	Detector	Description
1	0VBA	V0	signal in V0A in Beam-Beam
2	0VBC	V0	signal in V0C in Beam-Beam
3	0TVX	T0	T0-vértice (T0 vertex)
4	0UBA	AD	signal in ADA in Beam-Beam
5	0UBC	AD	signal in ADC in Beam-Beam
6	0SMB	SPD	SPD minimum bias single
7	0V0M	V0	
8	0ZED	ZDC	
9	0VSC	V0	
10	0V0H	V0	
11	0T0A	T0	A was hit
12	0OM2	TOF	At least 2 TOF pads triggered
13	0OMU	TOF	Between 2 and 6 TOF pad triggered
14	0BPA	BPX	bptx A–side
15	0BPC	BPX	bptx C–side
16	0STG	SPD	SPD topological trigger with optional opening angle
17	0MSH	MTR	
18	0MLL	MTR	like sign di-muon low threshold
19	0MUL	MTR	unlike sign di-muon low threshold
20	0MSL	MTR	single muon low threshold
21	0PH0	PHOS	PHOS level 0
22	0EMC	EmCal	EMCal level 0
23	0DMC		
24	0LSR	Laser	Hardware calibration trigger

TABLE 4.2: L0 trigger inputs active in Pb-Pb runs for 2018

4. Detector cluster

5. Rare flag(optional)

So, a generic name for a trigger could be write as: C[descriptor code]–[bunch crossing mask code]–[past–future protection code]–[detector cluster code]–[rare flag]. An example is CINT7-A-NOPF-CENTNOPMD, where "INT7" is the descriptor, "A" the bunch crossing mask code , NOPF is the past future protection code, for this case NOPF means that no past future protection was applied, CENTNOPMD is the cluster code and there are not rare flags. Each trigger class has six counters, L0b, L0a, L1b, L1a, L2b and L2a, where b and a stand for before and after. L0b gives the number of times a trigger class is counted and L2a gives the number of times the same trigger class passes the CTP and detector dead–time, and other possible vetos like downscaling.

Input ID	Input Name	Detector
1	1EJ1	EmCal
2	1EG1	EmCal
3	1EJ2	EmCal
4	1EG2	EmCal
5	1PHL	PHOS
6	1PHM	PHOS
7	1PHH	PHOS
9	1HCO	TRD
10	1HJT	TRD
11	1HSE	TRD
12	1H12	TRD
13	1HQU	TRD

Input ID	Input Name	Detector
14	1HNU	TRD
15	1ZED	ZDC
16	1ZMS	ZDC
17	1ZMB	ZDC
18	1ZNC	ZDC
19	1ZAC	ZDC
20	1DJ1	
21	1DG1	
22	1DJ2	
23	1DG2	

TABLE 4.3: L1 trigger inputs active in Pb-Pb runs for 2018(from ALICE Logbook)

4.7 ALICE GRID

The GRID of the ALICE experiment is a Worldwide Computing Network which is designed to share computing power and storage capacity over the Internet. Under normal conditions, the LHC experiment produces about 600 million collisions / second, which translates to about 15 Petabytes of information per year, and currently there is no way to store all that information in one place, so it is necessary distribute them in different places and also support them. The Grid connects computers distributed throughout the world, and also allows access to the resources of the connected computers. These resources include data memory, process power, sensors, visualization tools among others, on the other hand, the World Wide Web allows access to the information hosted on these computers. The Grid can combine the resources of thousands of computers to create a powerful resource, accessible from the comfort of a personal computer and useful for multiple uses in science. The Grid is based on fiber optic networks dedicated to distributing data from CERN to eleven major computing centers in Europe, North America and Asia. Of these, the data is sent to more than 140 centers in 33 countries: Australia, Austria, Belgium, Canada, China, the Czech Republic, Denmark, Estonia, Finland, France, Germany, Hungary, Italy, India, Israel, Japan , Republic of Korea, the Netherlands, Norway, Pakistan, Poland, Portugal, Romania, the Russian Federation, Slovenia, Spain, Sweden, Switzerland, Taibei, Turkey, the United Kingdom, Ukraine, and the United States of America. The distribution of data around the world is based on a model of 4 levels, labeled from 0 to 3. Each level is made up of several computer centers that provide a specific set of services. Level 0 is the CERN data center, in which a first backup is stored, which includes all the raw data taken by the detectors during collisions, and at this level the first steps are carried out for the conversion of these raw data into data with physical information.

Level 1 is made up of large computing centers, which also have large storage capacities, and provide 24-hour support for the GRID, here also raw and reconstructed data is stored and processed on a large scale. Level 1 centers allow access to data to Level 2 centers which consist of one or more associations of computer facilities that can store enough data and provide adequate processing speed for data analysis tasks, usually they are universities or universities. other research centers, and finally scientists can access data from previous levels through level 3, which can consist of a local cluster, a university department or even a personal computer.

4.7.1 Analysis on the GRID

The analysis framework for the ALICE experiment is AliROOT, which is based on the software packges ROOT and GEANT. AliRoot uses the ROOT system as a foundation on which the framework for simulation, reconstruction and analysis is built. ROOT is an object oriented software framework for high energy physics and provides a basic set of features and tools. ROOT is written in and heavily relies on the C++ programming language. GEANT is a toolkit that describes the passage of elementary particles through matter

The analysis framework in AliRoot makes it possible for users to analyse large data sets. The analysis is done with analysis tasks based in C++.

To access the GRID from a personal computer, it can be done by loading the variables of the alien environment (that includes AliROOT), for this a certificate granted by CERN to members of the experiment is needed. Once inside, what is done to obtain information about the collisions is to launch "jobs", a job is part of the GRID resources and is in charge of gathering the data required for a particular study along with the physical information that we request of those data. To launch the jobs an analysis task is required. In the analysis task the data to be collected is specified, and also a first(or a complete) data analysis could be carried out through the same analysis task. Once the job is finished information can be downloaded. The output is usually data structures called Trees, which contains event and track information for the selected events. The information of the tree can be further analysed offline.

4.7.2 ALICE Logbook

In large experiments like ALICE, it is necessary to have a tool to keep records of the activities carried out, in such a way that it is easy to access these records. ALICE has a central repository called "ALICE Electronic LogBook", in which reports of incidents, changes in the configuration of the experiment, and of course, information on the data collected and validated by the firing systems during particle collisions are stored. which can be downloaded for further study This application developed for the ALICE experiment was implemented by the ALICE data acquisition team (DAQ) since 2007.

A run is a period of time during which collisions between particles are recorded in the LHC, either protons or heavy ions, depending on the objective of said run, and in which all or only some of the detectors can intervene, again, depending on the type of physical processes that are pursued. The runs can last from minutes to several hours, this is usually determined by how long the detectors work correctly. The whole information of each run, such as the type of collision, the energy at which the particles are made to collide, the events collected and reconstructed, detector failures, etc., is registered in the ALICE logbook. The runs are grouped into periods denoted by letters of the alphabet, the runs per period can vary and the duration of each period as well, although on average it is approximately 1 month per period. The selection of runs suitable for a study is done through the Logbook.

Chapter 5

Data Analysis

In this chapter the data selection an analysis for Pb-Pb collisions data samples corresponding to the year 2018 are presented. The two systems, $\pi^+\pi^-$ and $\pi^+\pi^-\pi^+\pi^-$ are studied. First, the data samples for both studies are given in section 7.2, the event selection is presented in section 7.3, the analysis for the $\pi^+\pi^-$ case is presented in section 7.4, and the analysis corresponding to $\pi^+\pi^-\pi^+\pi^-$ in section 7.6. Acceptance and efficiency corrections for the 2 and 4 pions case is presented in sections 7.5 and 7.7 respectively.

5.1 Reconstruction of kinematic variables

The primary objective of the analysis is to reconstruct an invariant mass spectrum of the "mother" particles created immediately after the collision and that cannot be detected due to their short lifetime, but that can be studied through the particles(pions) they decay in.

5.1.1 4-momenta reconstruction

The 4-momenta of a mother "M" particle that decays into 2 pions can be reconstructed as follows:

$$p^{\mu}_{M} = p^{\mu}_{\pi^+} + p^{\mu}_{\pi^-} \tag{5.1}$$

if M decays into 4 pions, then:

$$p^{\mu}_{M} = p^{\mu}_{\pi^+} + p^{\mu}_{\pi^-} + p^{\mu}_{\pi^+} + p^{\mu}_{\pi^-} \tag{5.2}$$

where $p^{\mu}_{\pi^+}$ and $p^{\mu}_{\pi^-}$ in 5.1 and 5.2 denote the 4-momenta of the positively charged pion and the the 4-momenta of the negatively charged pion respectively. The first component of the 4-momenta is the energy, which in this case is obtained from the moment and the mass of the pions, and in turn, the moment is obtained through the measurements of the ITS, TPC and TOF detectors.

5.1.2 Invariant mass reconstruction

The invariant mass of a particle X decaying into another particles can be reconstructed from the 4-moment sum of such particles, taking into account that the 4-moment of a particle fulfills that:

$$p^{\mu}_{M} p^{\mu}_{M} = {m_x}^2 \tag{5.3}$$

Therefore, according to 5.1 and 5.2, the invariant mass for the 2 will be:

$$m_M = \sqrt{(p^\mu_{\pi^+} + p^\mu_{\pi^-}) \cdot (p^\mu_{\pi^+} + p^\mu_{\pi^-})} \tag{5.4}$$

And for the 4 pions decay;

$$m_M = \sqrt{(p^\mu_{\pi^+} + p^\mu_{\pi^-} + p^\mu_{\pi^+} + p^\mu_{\pi^-}) \cdot (p^\mu_{\pi^+} + p^\mu_{\pi^-} + p^\mu_{\pi^+} + p^\mu_{\pi^-})} \tag{5.5}$$

5.2 Data Samples

In 2018 at ALICE, lead-lead collisions took place in November during the LHC18q and LHC18r periods, at a center of mass energy of $\sqrt{S_{NN}}$ =. The run range is 295530-297635.

5.2.1 Triggers in 2018 (Central Barrel)

The triggers defined for UPC in Pb-Pb collisions during 2018 in the central barrel are:

- CCUP29-B-NOPF-CENTNOTRD = *0VBA *0VBC *0UBA *0UBC 0STG
- CCUP30-B-NOPF-CENTNOTRD = *0VBA *0VBC *0UBA *0UBC 0STG 0OM2
- CCUP31-B-NOPF-CENTNOTRD = *0VBA *0VBC *0UBA *0UBC 0STG 0OMU

where the trigger elements are defined as:

- *0VBA = No signal in V0A in BB window
- *0VBC = No signal in V0C in BB window
- *0UBA = No signal in ADA in BB window
- *0UBC = No signal in ADC in BB window
- 0STG = SPD topological trigger with optional opening angle
- 0OMU = Between 2 and 6 TOF pad triggered
- 0OM2 = At least 2 TOF pads triggered

Starting from run 295881 past-future protection for SPD was introduced due to high trigger rate:

- SPD2 = protection in 6 previous bcs
- CCUP29-B-NOPF-CENTNOTRD (downscaled $\sim$ 0.1%)
- CCUP29-B-SPD2-CENTNOTRD (downscaled $\sim$ 0.1%)

- CCUP30-B-SPD2-CENTNOTRD (downscaled $\sim$ 5%)
- CCUP31-B-NOPF-CENTNOTRD (downscaled $\sim$ 5%)
- CCUP31-B-SPD2-CENTNOTRD (fully open)

The main trigger used in this study is the CCUP31-B-SPD-CENTNOTRD, we will refer to it simply as CUP31 from now on.

5.2.2 Runs

The run selection was done through the ALICE electronic Logbook, the repository designed to store data from the ALICE experiment. The suitable runs are those that meet the following requirements:

- Runs from LHC18r or LHC18q period
- Run type: Physics
- At least 1 CUP31 trigger at L2a level
- Quality flag "Not bad run" for the SPD, V0, AD and TOF detectors.
- Quality flag "Good run" for the TPC detector.

A total of 192 runs met the requirements, 89 for the LHC18q period and 103 for the LHC18r period. To be sure the main detectors used in this study worked well, the status at the run condition table for the detectors TPC,TOF,V0 and SPD in MonAlisa(The ALICE repository) was checked, and only the runs were these detectors are labelled as "Detector was ON and running according to nominal specifications" were used. In total 83 runs for the LHC18q period and 89 runs for the LHC18r were selected. The logbook registered 9312234 events triggered by CUP31 in these runs. In total 3 602 451 events were used for the $\pi^+\pi^-$ study and 1240425 events were used for the $\pi^+\pi^-\pi^+\pi^-$ study. The same runs are used for the two an four pions study.

The runs numbers are listed by period:

LHC18q

Run numbers used in this study for this period:
296623 296622 296619 296618 296616 296615 296553 296552 296551 296550 296549 296548 296547 296516 296512 296511 296510 296509 296472 296433 296424 296423 296420 296419 296415 296414 296383 296381 296380 296379 296378 296377 296312 296309 296304 296303 296280 296279 296273 296270 296269 296247 296246 296244 296243 296242 296241 296240 296198 296197 296196 296195 296194 296192 296191 296143 296142 296135 296134 296133 296132 296123 296066 296065 296063 296062 296060 296016 295942 295941 295937 295936 295913 295910 295909 295861 295860 295859 295856 295855 295854 295831 295829

The runs 295829 and 295831 had 560 colliding bunches, the runs 295854 to 295913 had 619, the runs 295936 to 296066 had 316, the runs 296123 to 296553 had 619, and runs 296615 to 296623 had 456.

LHC18r

297624 297595 297590 297588 297558 297544 297542 297541 297540 297537 297512 297483 297481 297479 297452 297451 297450 297446 297442 297441 297415 297414 297413 297406 297405 297380 297379 297372 297367 297366 297363 297336 297335 297333 297332 297317 297311 297310 297278 297222 297221 297218 297196 297193 297133 297132 297129 297128 297124 297123 297119 297118 297117 297085 297035 297031 296966 296941 296938 296935 296934 296932 296931 296930 296903 296900 296899 296894 296852 296851 296850 296848 296839 296838 296836 296835 296799 296794 296793 296790 296787 296786 296785 296784 296781 296694 296693 296691 296690

The runs 296690 to 296694 had 456 colliding bunches, runs from 296781 to 297278 had 702, runs from 297310 to 297336 had 619, runs from 297363 to 297595 had 702, runs 297624 and 297623 had 78.

5.3 Selection of events

5.3.1 Preselection

The analysis has been carried out using ESD pass 1 data of the runs listed above. The Analysis Task used for this study is based in the AliAnalysisTaskUpcRho0 class found in:

https://github.com/alisw/AliPhysics/blob/master/PWGUD/UPC/ AliAnalysisTaskUpcRho0.cxx
https://github.com/alisw/AliPhysics/blob/master/PWGUD/UPC/ AliAnalysisTaskUpcRho0.h

The only relevant modification done to the class for the 2 pions study is the addition of code that indicate whether the tracks had attached a TOF cluster.

The AliAnalysisTaskUpcRho0 has the following track requirements:

- The track must be a track refitted in both TPC and ITS
- TPC clusters > 50
- TPCχ^2/TPCclusters< 4
- The track must come from a reconstructed primary vertex
- 2 hits on ITS layers 0 and 1 (SPD layers)matched to the track.
- Distance of closest approach to the primary vertex below 2cm in the z axis and below $0.0182 + 0.035/Pt^{1.01}$ in the xy plane.

Furthermore the class select only those events where exist exactly two good tracks, and store the required information of this events:Pt momentum, rapidity η, azimuth angle ϕ, energy deposed in ZDC,PID provided by TOF, tracks that reached TOF, electric charge, VO and AD offline decisions.

Additionally the information about the triggers is stored, in particular whether the CUP31 trigger were activated in such events.

For the 4 pions study the same class is used, just changes the requirement in the number of tracks; 4 good tracks are required instead.

5.3.2 Offline event selection for $\pi^+\pi^-$ study

The suitable events for the 2 pion study need to fulfill the following conditions:

- Trigger CUP31 must have been activated
- The pair of tracks must have opposite charge sign.
- PID(particle identification): To ensure the particles we are treating are pions the following requirement in the standard deviations are required: $(\sigma_{\pi_1})^2 + (\sigma_{\pi_1})^2 < 4^2$, the $\sigma's$ are provided by TPC
- The V0 and AD offline decisions in both sides (A and C) must be "Empty", this will be better explained in the next section.
- Tracks must have attached a TOF cluster.
- Tracks emerge from a primary vertex located between $\pm 10cm$ in z direction of the ideal interaction point.
- The number of SPD Tracklets must be equal to two

For each of the 2 particles (positive and negative) a 4-vector is made from the transverse momentum of the track(pT), the azimuth angle(ϕ), the pseudorapidity η, and the assumption that the particle has the pion mass of $139.57061 \pm 0.00023MeV$ as reported in the PDG. Another 4-vector can be defined from the sum of the two 4-vectors mentioned, giving as result the 4-vector of the "Mother" particle which decay in two pions.

Kinematics requirements for the Mother particle:

- Rapidity $y < 0.9$ (TPC acceptance)
- Transverse momentum in the coherent zone ($pT < 150MeV$)

5.3.3 Offline event selection for $\pi^+\pi^-\pi^+\pi^-$ study

The suitable events for the 4 pion study need to fulfill similar conditions as for the 2 pions case:

- Trigger CUP31 must have been activated
- 4 tracks charge sum must be identically equal to zero
- PID: To ensure the particles we are treating are pions The following requirement in the standard deviations are required: $(\sigma_{\pi_1})^2 + (\sigma_{\pi_2})^2 + (\sigma_{\pi_3})^2 + (\sigma_{\pi_4})^2 < 4^2$, the $\sigma's$ are provided by TPC
- V0 and AD offline decisions in both sides (A and C) must be "Empty"
- Tracks must have attached TOF cluster(at least two tracks).
- Tracks emerge from a primary vertex located between $\pm 10cm$ in z direction of the ideal interaction point.

Data selection	Number of events
Events triggered by CUP31	3 602 451
Events with opposite charge tracks	2 312 174
PID TPC	2 061 835
Vertex	1 942 392
rapidity	1 933 808
V0 decision	1 256 870
AD decision	1 234 012
Number of tracklets	478 248
Pt	249 368
two tracks reaching TOF	35 195

TABLE 5.1: 2-tracks events after data selection

In the same way, for each of the 4 particles a 4-vector is made from the transverse momentum of the track(pT), the azimuth angle(ϕ), the pseudorapidity η, and the assumption that the particle has the pion mass of $139.57061 \pm 0.00023 MeV$ as reported in the PDG. Another 4-vector can be defined from the sum of the four 4-vectors , giving as result the 4-vector of the "Mother" particle which decay in four pions.

Kinematics requirements for the Mother particle:

- Rapidity $y < 0.9$ (TPC acceptance)
- Transverse momentum in the coherent zone ($pT < 150 MeV$)

5.4 $\pi^+\pi^-$ Analysis

As pointed out before, 3602451 events out of 9312234 registered in the logbook for the CUP31 trigger were used for the $\pi^+\pi^-$ study. These events fulfilled the requested requirements in the logbook and by the class AliAnalisysTaskUPCRho0, and conform our preselected data. In this section such preselected data is analysed, the offline data cuts are better explained and the distributions of relevant variables for this study are presented.

In table 5.1 the number of events after every data cut is presented.

5.4.1 Tracks properties

The pT, pesudorapidity and azimuth angle for the individual tracks is shown in figure 5.1. The only requirements for the tracks(besides those of the preselection stage) are that they muust come come from events where the trigger CUP31 has been activated and have opposite sign charge

5.4.2 Primary Vertex

The vertex distribution in z direction is shown in figure 5.2. for events triggered by CUP31 and with opposite sign tracks. In ALICE a primary vertex is

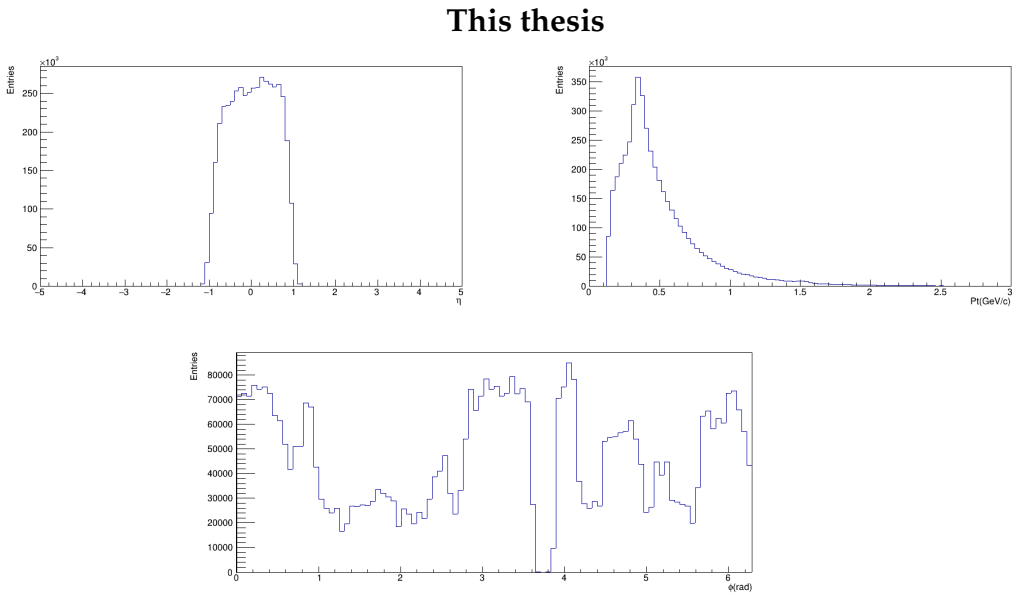

FIGURE 5.1: Tracks properties

taken to be valid when it is located between $\pm 10cm$ of the interaction point. The figure show that most of the events come from a vertex in the accepted region.

5.4.3 Particle Identification by TPC

The TPC provides information for particle indentification by measuring the energy loss dE/dx, charge and the momentum p of particles that pass through it. The energy loss, described by Bethe-Bloch formula, is parameterized by [16]:

$$f(\beta\gamma) = \frac{P_1}{\beta^{P_4}}\left(P_2 - \beta^{P_4} - \ln\left(P_3 + \frac{1}{(\beta\gamma)^{P_5}}\right)\right) \tag{5.6}$$

where β is the particle velocity, γ the Lorentz factor and the P's are fit parameters.

The dE/dx shape is well distinguished for different particles species (π, p, K, e, μ) and can be fitted to a Gaussian. The TPC provides information about the number of $\sigma's$(standard deviations) the measured particle is of the expected value to be a π, p, K, e or μ.

For this study only the pair of tracks with more probability of correspond to pions are taken into account, it is done applying the PID cut described in section 4.2. In figure 5.3 the TPC signal (dE/dx) vs the track momentum is shown before an after the PID cut; it is clearly seen how contamination from protons, electrons and kaons is removed after this data cut. In the same figure is shown the σ distribution of track 1 versus the σ distribution of track 1 before and after the PID cut, an is seen the data portion used is the data enclosed by a circle of radius 4σ.

This thesis

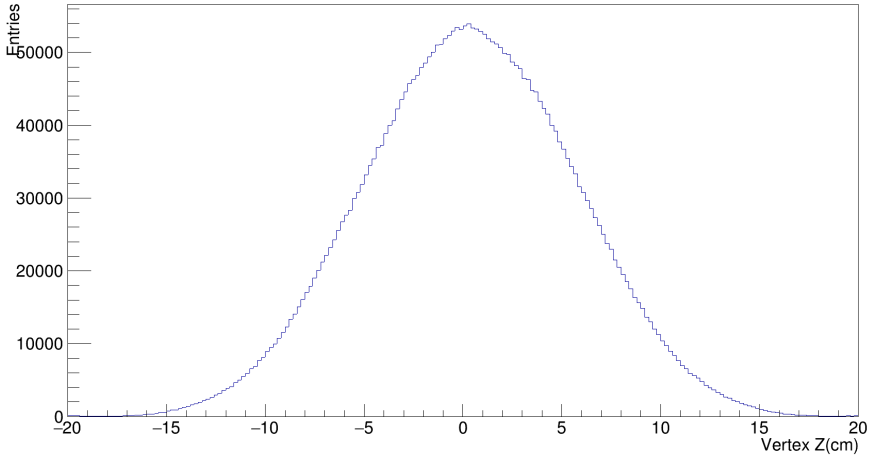

FIGURE 5.2: Z vertex

This thesis

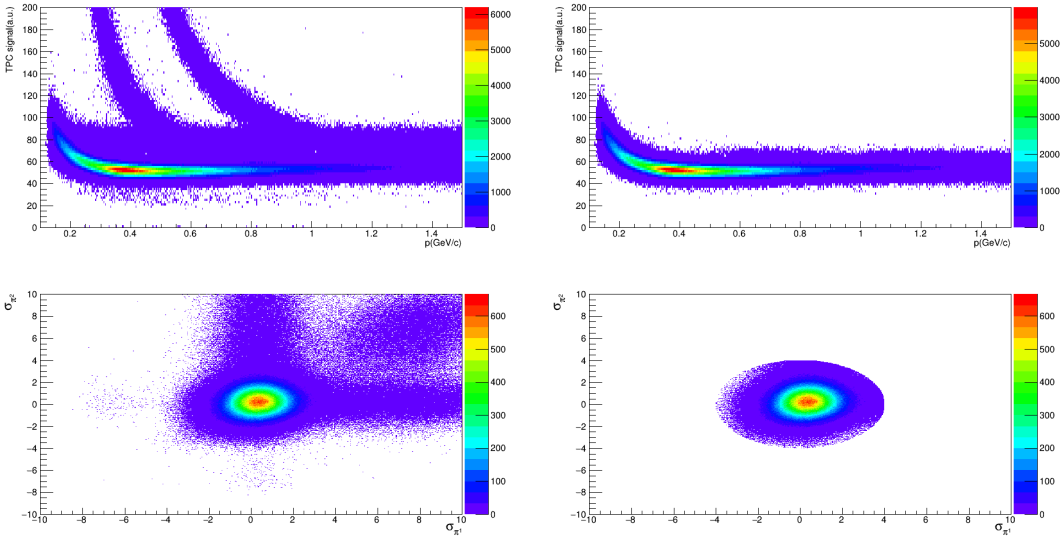

FIGURE 5.3: TPC signal vs momentum of the individual tracks(up-left), TPC signal vs momentum after pid cut(up-right)), σ provided by TPC for particle 1 vs σ of particle 2(Bottom-left), σ for particle 1 vs σ of particle 2 after pid cut(Bottom-left). Discussed in [32]

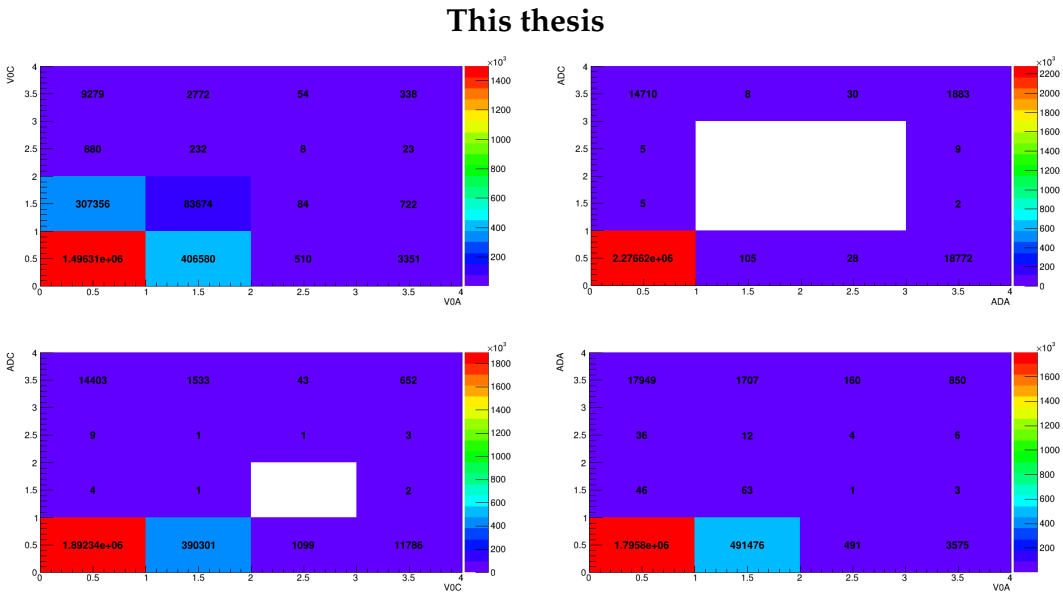

FIGURE 5.4: V0 offline decisions(up-left), AD offline decisions()up-right,V0C decisions compared with ADC decisions(bottom-left), V0A decision compared with ADA decisions(bottom-right). [32]

5.4.4 V0 and AD decisions

The V0 and AD detectors allow to characterize the event interactions through its corresponding offline decisions which are labelled from o to 3. The meaning of the decisions is:

- 0 = Empty : the detector is empty
- 1= Beam-Beam: the beam A interacted directly with beam C
- 2= Beam-Gas: the beam (A or C) interacted with the gas in the tube.
- 3: Fake: a fake signal in the detector.

For this study the offline decision for V0 and AD was required to be "Empty" in order to avoid central collision events that occur in beam-beam interactions.

The offline decisions for the V0 and AD are shown in figure 5.4, in the same figure a comparison between the V0 and AD decisions is presented.

5.4.5 Tracklets

The reconstructed points of the SPD (clusters) and the reconstructed primary vertex position are used to build tracklets. A condition on the number n of tracklets (n = 2) helps to decrease the incoherent background without significantly reducing the coherent region statistics, the effect of this condition is clearly seen in the pT distribution shown below. In figure 5.5 the number of tracklets from events triggered by CUP31 and with opposite charge tracks is shown.

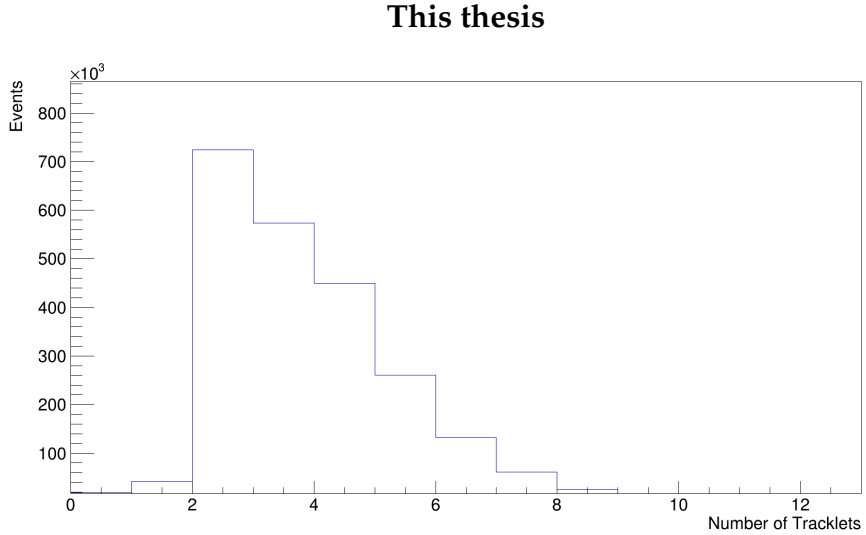

FIGURE 5.5: Number of Tracklets. Discussed in [37]

5.4.6 Transverse momentum distribution

The transverse momentum distribution(after the trigger,charge, PID, and V0-AD decisions data cuts) for the reconstructed mother particle is shown in figure 5.6. A peak is clearly seen in the coherent region, below 0.1 GeV. The events in the not coherent section come from the incoherent production of th ρ^0, and its contribution to the coherent region can be estimated with Monte Carlo simulations. The second pt distribution in figure 5.7 show the effect of the condition on the number of tracklets to reduce incoherent background.

5.4.7 Uncorrected invariant mass distribution

The invariant mass distribution (after all data cuts but TOF condition) for the reconstructed mother particle is shown in figure 5.8.In figure 5.9 the invariant mass distribution including the condition that two tracks must reach the TOF with angular condition is added. No efficiency or acceptance corrections are made yet.

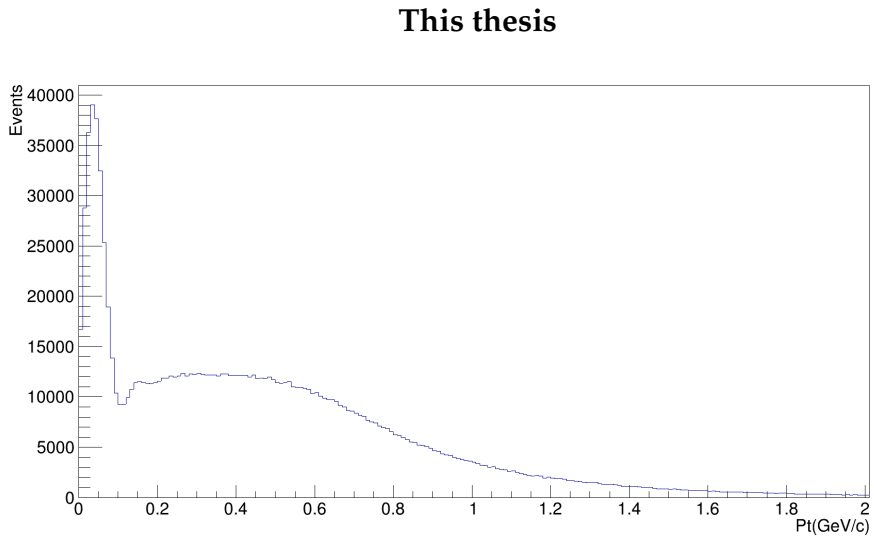

FIGURE 5.6: Pt distribution. Discussed in [37, 32, 33]

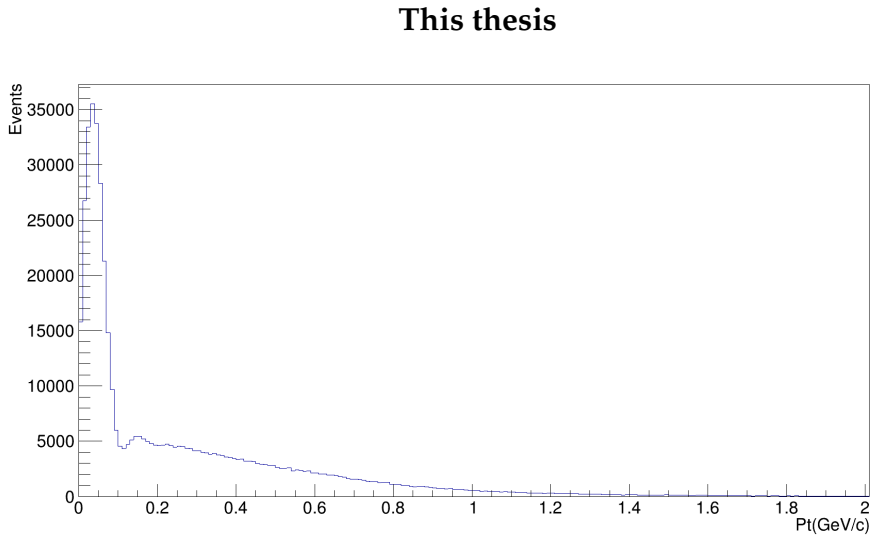

FIGURE 5.7: Pt distribution with condition over the number of tracklets. Discussed in [37, 32, 33]

5.5 Acceptance and efficiency corrections $\pi^+\pi^-$

The $\pi^+\pi^-$ invariant mass distribution needs to be corrected for detector acceptance and efficiency. The acceptance is related to the geometry and active areas of the detectors; an event whose particles have trajectories outside the detection area will be rejected. The acceptance is defined as the ratio of the number of events where the two tracks hit the detectors active areas to the number of events with two tracks. The detectors are not 100% efficient, that is, the tracks(and other properties as the mass or the dE/dx) of particles hitting them won't be measured accurately all the time, or may not be measured at all, so ,not all particles that goes through the detectors will be reconstructed. The

This thesis

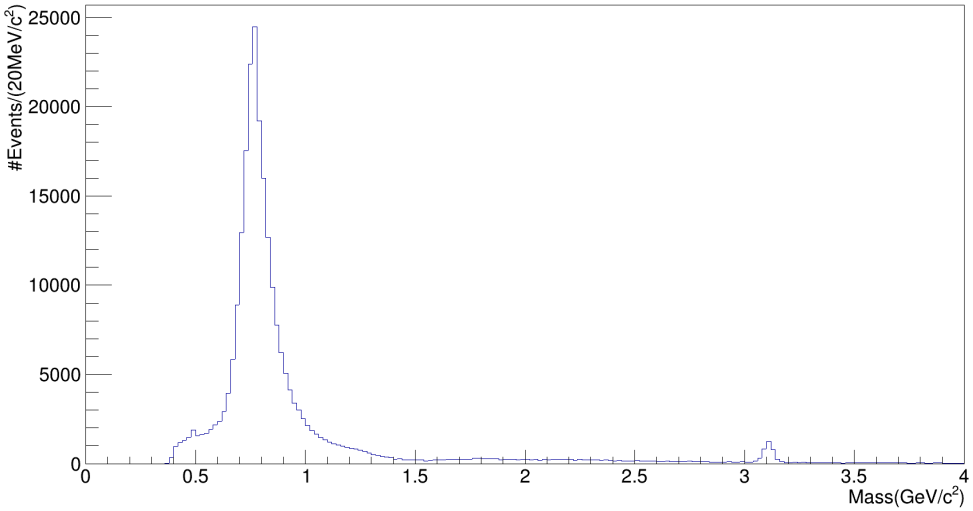

FIGURE 5.8: $\pi^+\pi^-$Invariant mass distribution. Discussed in [33, 35, 36, 38, 37]

This thesis

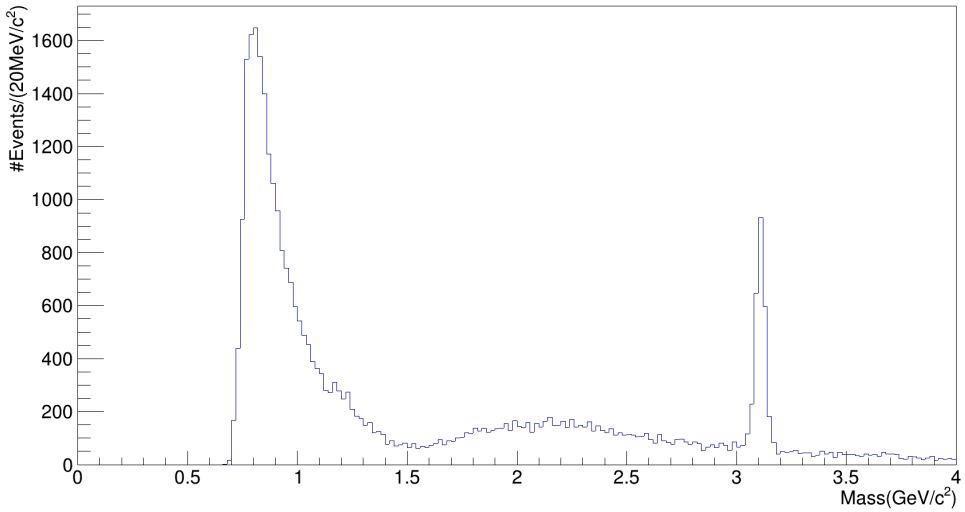

FIGURE 5.9: $\pi^+\pi^-$Invariant mass distribution with tracks reaching TOF.Discussed in [33, 35, 36, 38, 37]

reconstruction efficiency is the ratio of the number of particles reconstructed to the to the number of particles traversing the detectors. The total efficiency, or rather (Acc x Eff), is the product of the acceptance of the detector and the reconstruction efficiency, which can be seen also as the ratio of two-track events reconstructed to the total number of events where a ρ^0 was photoproduced. For a MC sample:

$$Acc \times Eff = \frac{N_{Rec}}{N_{Gen}} \tag{5.7}$$

where N_{Rec} is the number of reconstructed events after the data selection and N_{Gen} is the number of generated events.

5.5.1 Simulation of a ρ^0 like mass distribution

In order to estimate the $Acc \times Eff$ a Monte Carlo(MC) simulation is used. The event generator is STARLIGHT, the simulated process is the labelled as kCohRhoTopi, which corresponds to simulation of a coherent ρ^0 sample with a breit-wigner invariant mass distribution. The rapidity of the generated ρ^0 was restricted to the region $-1 < y < 1$, the mass range is $2m\pi \leq M \leq 1.525 GeV/c^2$, and the transverse momentum $p_T < 0.15 GeV/c$. The simulation is anchored to the run 296377. Detector conditions may vary from one run to another, the information about the detector status is stored for each run in the OCDB(Offline Conditions Data Base). The OCDB information for the run 296377 is used during the simulation in order to reproduce the exact conditions of the detector.

The generated events passed through an ALICE Geant simulation and then through the same analysis procedures of data. The trigger CCUP31 is not simulated during the process, but information from the detectors after the simulation is used to emulate the conditions of the trigger and select only the reconstructed events that fulfill the trigger criteria.

In figure 5.10 the invariant mass distributions for the generated and reconstructed ρ^0 invariant mass simulation is shown for run 296377. The $Acc \times Eff$ calculated is shown in figure 5.11. The trigger CUP31 require that two tracks reach to the TOF, and that causes the Eff goes to zero around $500 MeV/c^2$; The TOF only measures pions with momentum of $\approx 300 MeV/c$ or higher.

The invariant mass distribution of $\pi^+\pi^-$ (figure 5.9), is corrected for acceptance and efficiency bin by bin. Because of the low efficiency, and therefore large errors, below $0.65 GeV/c^2$ and above $1.1 GeV/c^2$, only bins from $0.65 GeV/c^2$ to $1.1 GeV/c^2$ are corrected. The corrected invariant mass distributions can be seen in Figure 5.12.

5.6 $\pi^+\pi^-\pi^+\pi^-$ Analysis

A total of 1240425 events were used for the $\pi^+\pi^-\pi^+\pi^-$ analysis from the preselected data. In the same way as in the 2 pions case, in this section the distributions of relevant variables is presented as well as the results for the invariant mass reconstructed.

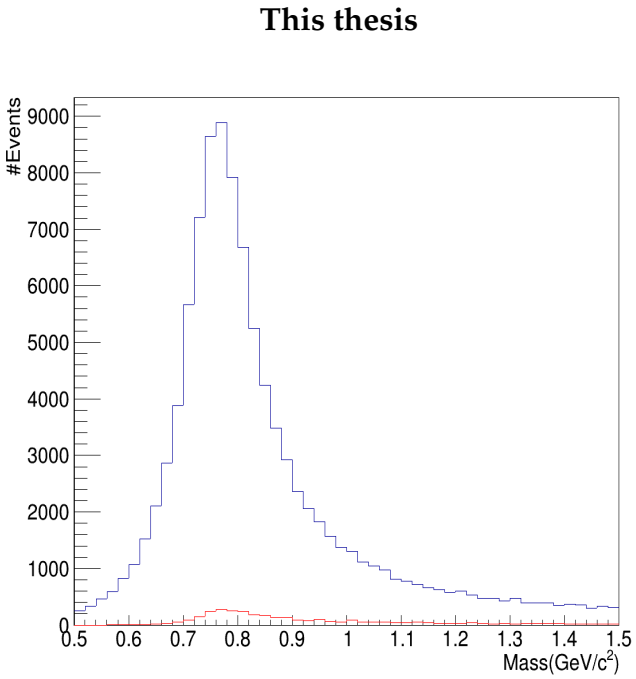

FIGURE 5.10: Number of Generated events(Blue) and number of reconstructed events in the rapidity range $-1 \leq y \leq 1$ and mass range $2m\pi \leq M \leq 1.525 GeV/c^2$ for run 296377

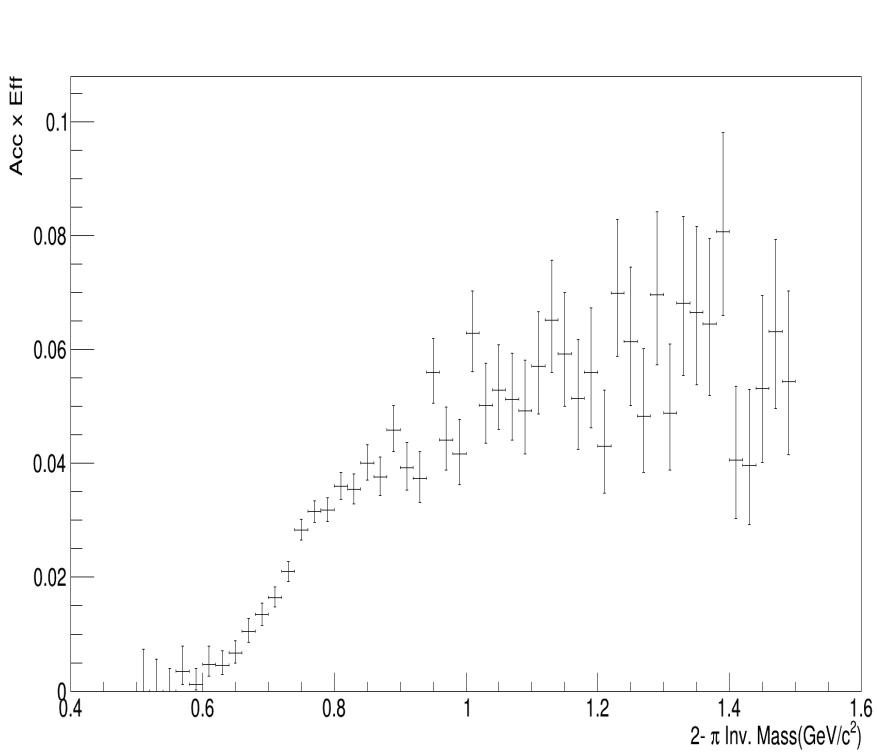

FIGURE 5.11: $(Acc \times Eff)$ for $\pi^+\pi^-$ production

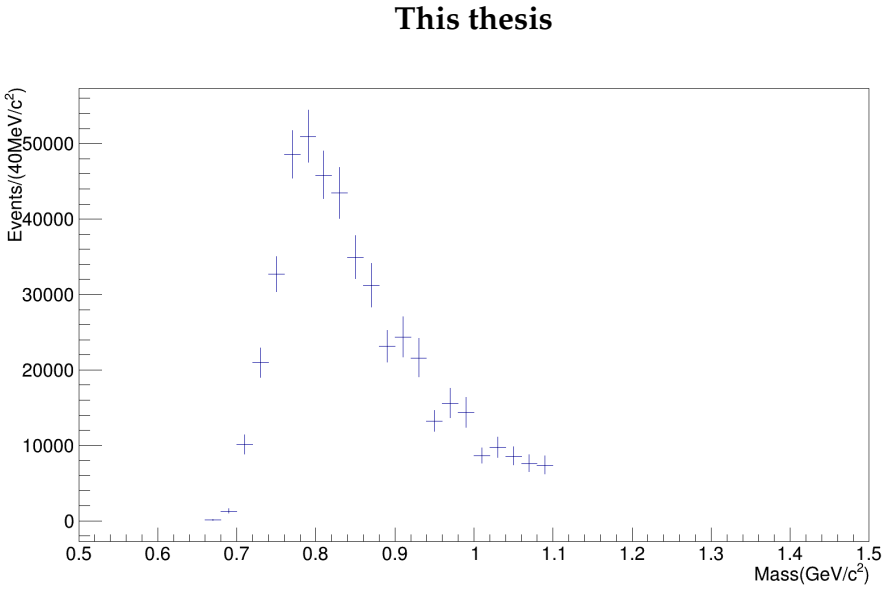

FIGURE 5.12: Corrected invariant mass 2-Tracks

In table 5.2 the number of events after every data cut is presented.

Data selection	Number of events
Events triggered by CUP31	1240425
Events with zero net charge	628318
PID TPC	504356
Vertex	481084
rapidity	480834
V0 decision	274982
AD decision	265039
Number of tracklets	74428
Pt	14010
At least two tracks reaching TOF	5744

TABLE 5.2: Events after data selection(4pions)

5.6.1 Tracks properties

The pseudorapidy, transverse momentum and azimuth angle distributions for the 4 tracks is shown in figure 5.13. The only requirements (besides those of the preselection) are that the tracks come from events where the trigger CUP31 has been activated and the total charge given by the sum of the individual tracks charge be equal to zero.

5.6.2 Vertex

In figure 5.14 the vertex distribution for the selected events is shown. Most of the data sample is in the desired region of $\pm 10cm$, though for this case the

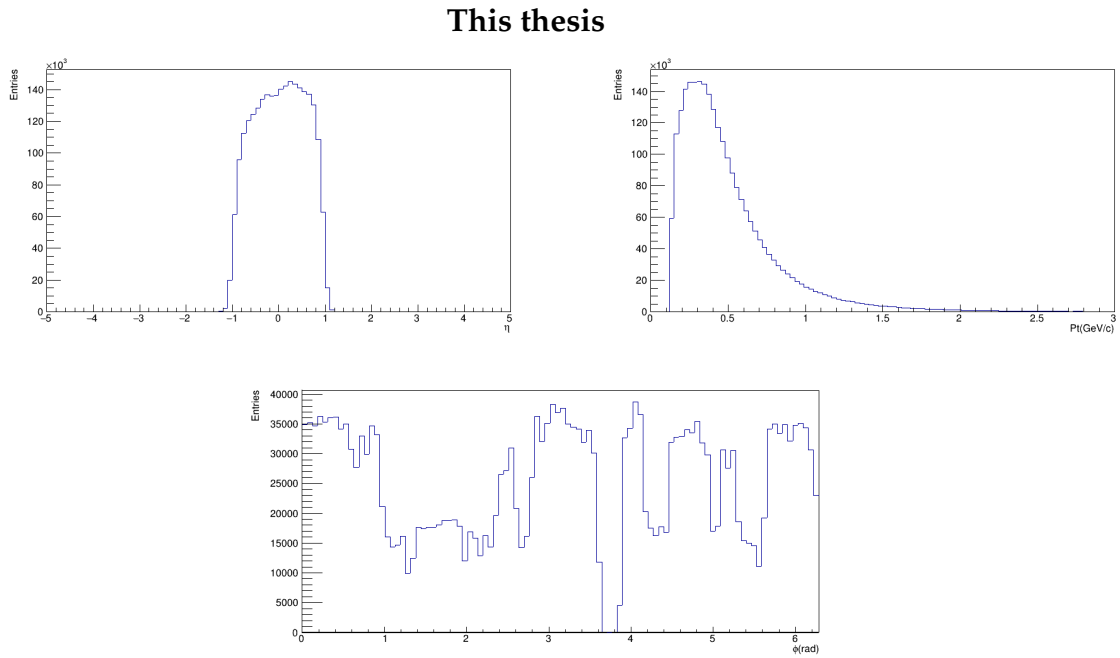

FIGURE 5.13: Individual properties 4 tracks

reconstructed vertex distribution exhibits a small enhancement in the positive region.

5.6.3 Particle identification

As with the 2 particles study, only tracks that had a higher probability of corresponding to a pion track were considered. In figure 5.15 we see the loss of energy vs the tracks momentum before and after the PID cut; it is also clear how contamination from protons, kaons and electrons is reduced. In figures 5.16 and 5.17 the correlation between the tracks $\sigma's$ before and after the PID cut can be seen.

5.6.4 AD and V0 offline decisions

The AD and V0 decisions are the same for this case; and an "Empty" signal is required in both V0 and AD detector.

5.6.5 Transverse momentum

The transverse momentum distribution(after trigger, charge,PID, vertex, rapidity, V0 and AD data cuts) is shown in figure 5.19. A clear peak can be seen in the coherent zone before approximately 120 MeV. In the same figure the pt distribution when the additional condition over the number of tracklets(n=4) is required. It can be clearly appreciated how the incoherent statistics decrease considerably with this requirement.

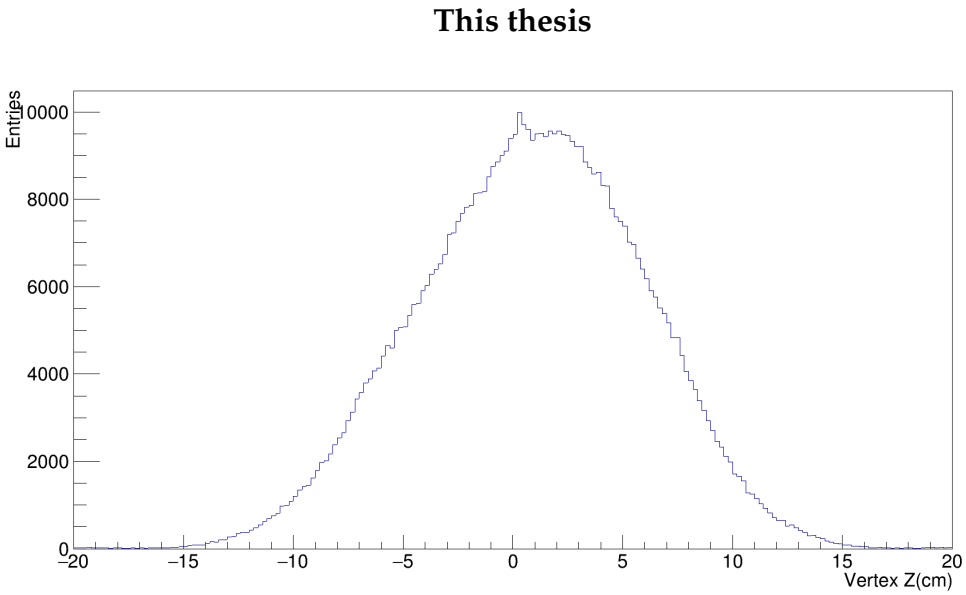

FIGURE 5.14: Z vertex 4 tracks

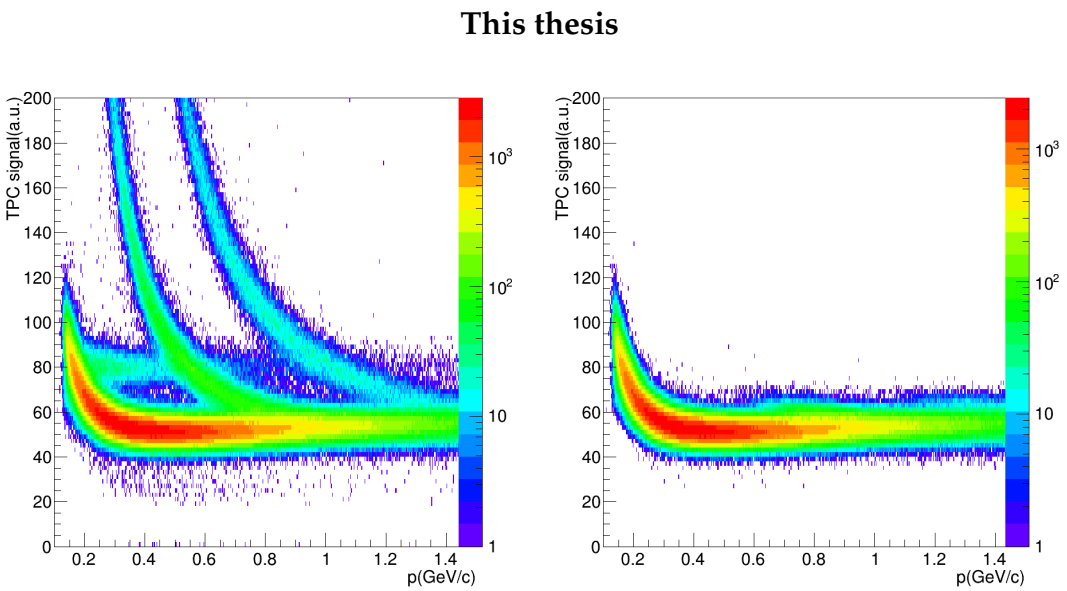

FIGURE 5.15: dE/dx vs track momentum before(left) and after(right) the PID cut.

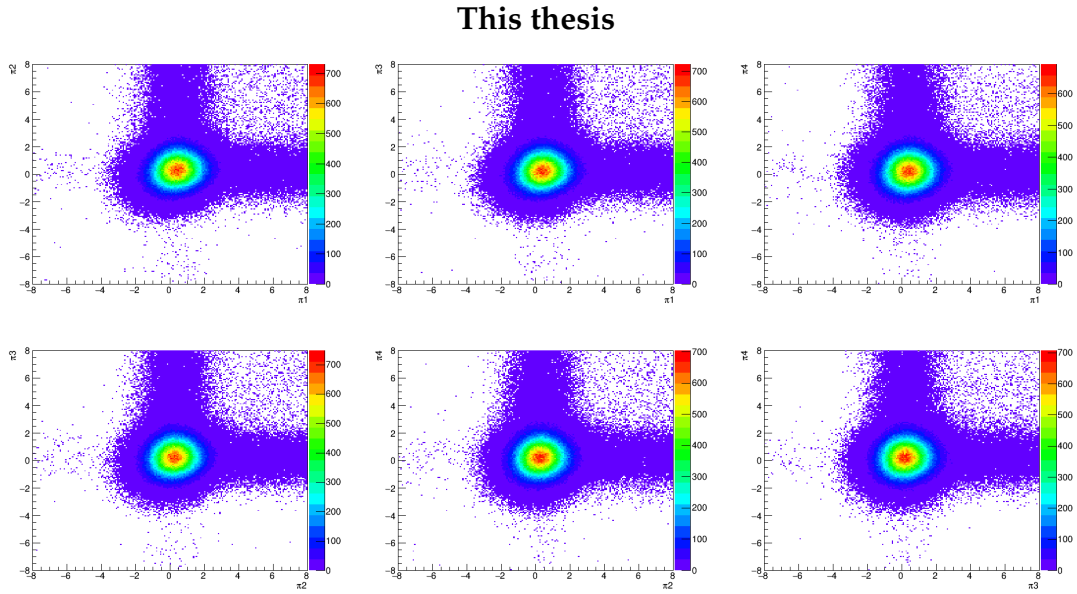

FIGURE 5.16: Correlation between the $\sigma's$ for the 4 tracks. Discussed in [33]

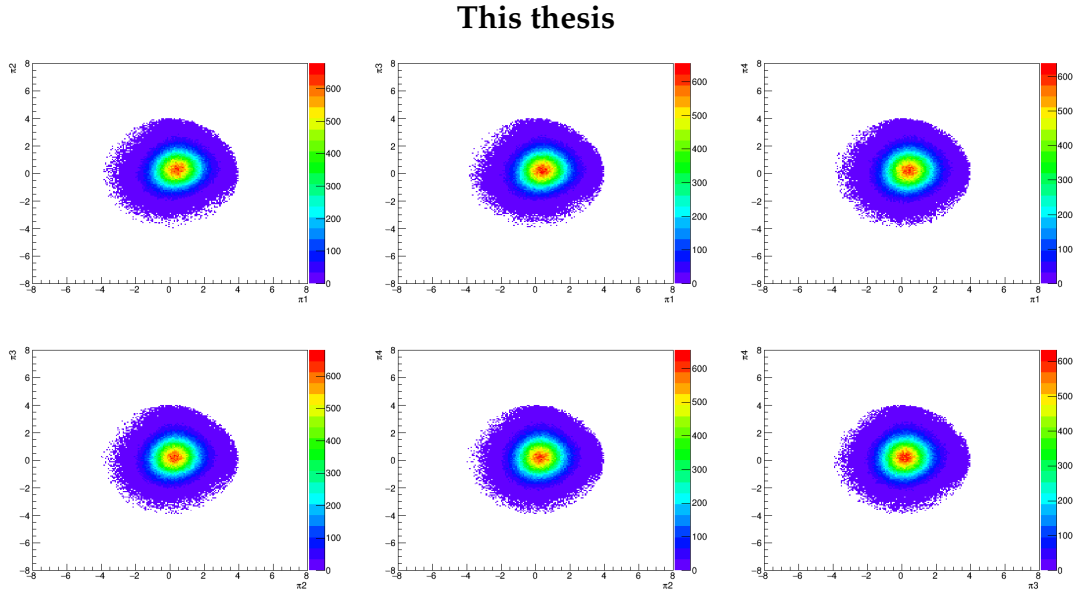

FIGURE 5.17: Correlation between the $\sigma's$ for the 4 tracks after PID cut. [33]

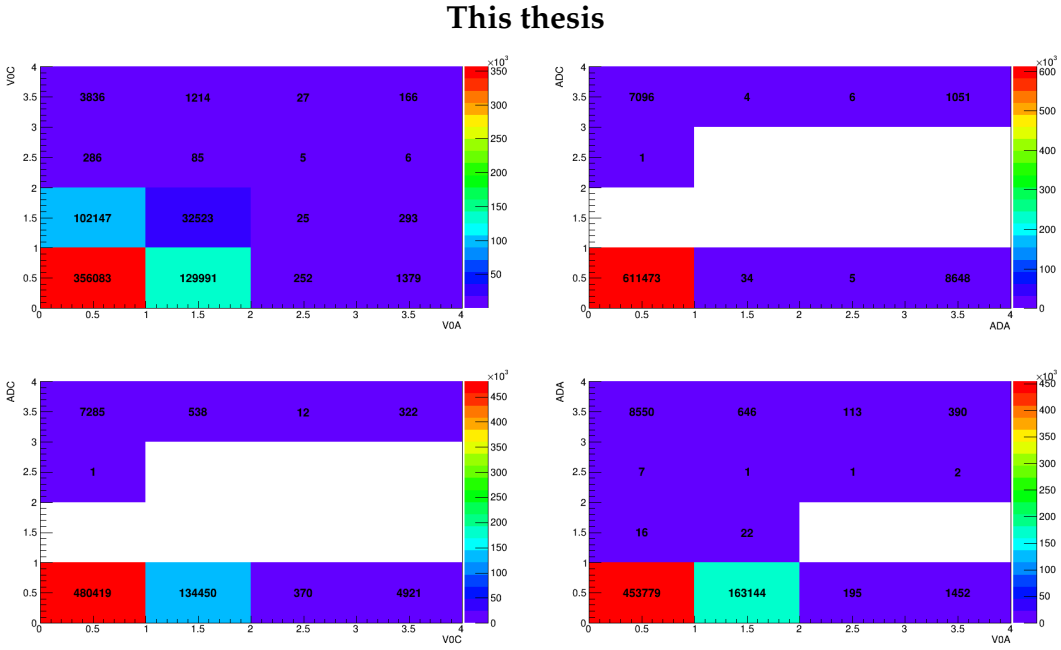

FIGURE 5.18: V0 and AD offline decisions. Discussed in [33]

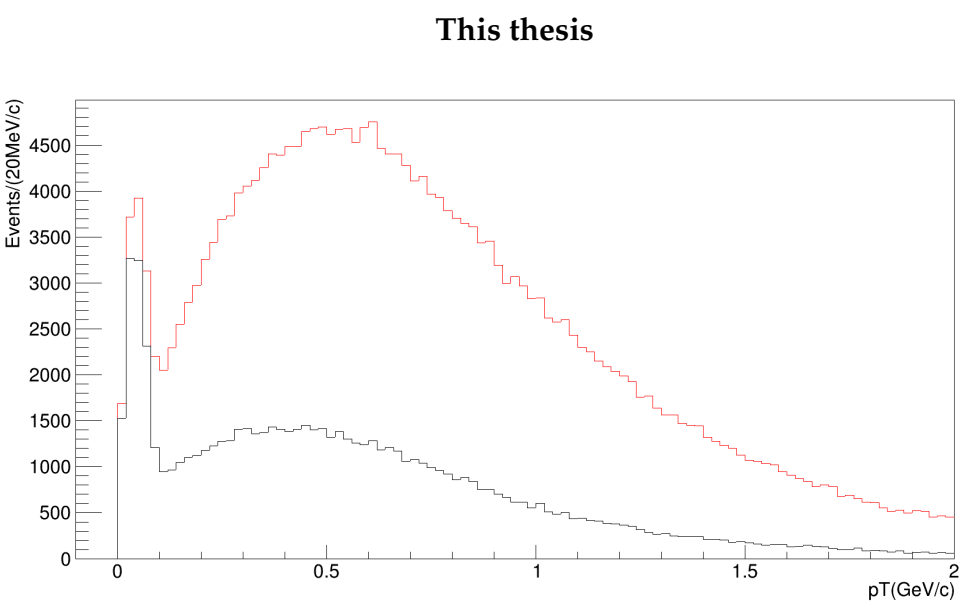

FIGURE 5.19: Transverse momentum. Discussed in [33, 32]

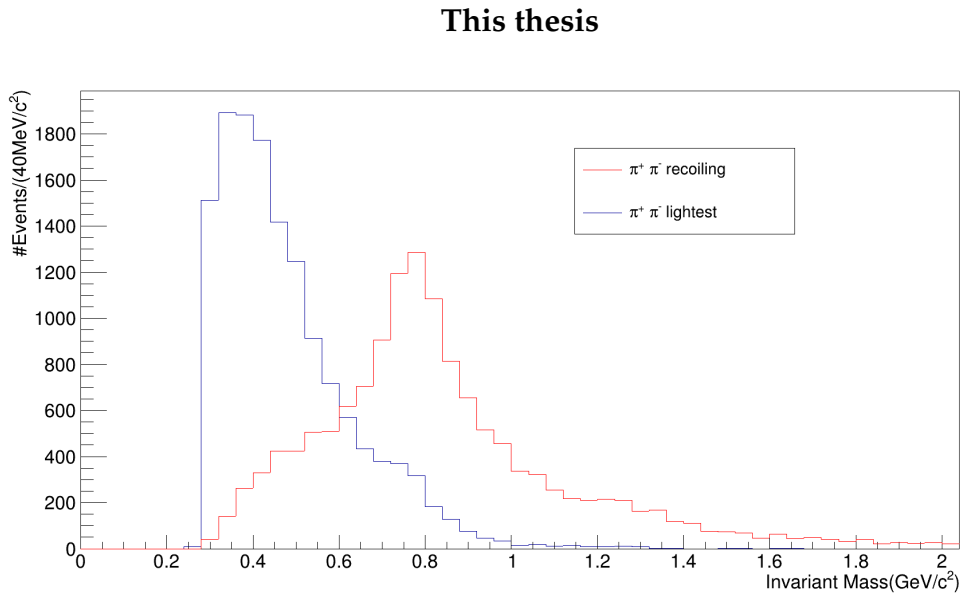

FIGURE 5.20: Invariant mass distribution of the 2-pion subsystems in collisions Pb-Pb in the ALICE experiment. The spectra of the heavier pair of pions (recoiling) exhibit a clear peak. Discussed in [33] in the region of the $\rho^0(770)$.

5.6.6 $\pi^+\pi^-$ subsystems

The invariant mass of each subsystem of 2 pions is shown in figure 5.20 with the pair of light pions (lightest) accompanied by $\rho^0(770)$ (recoiling).

5.6.7 Uncorrected invariant mass distribution

The reconstructed invariant mass distribution (after all data cuts but TOF condition) is shown in figure 5.21.In figure5.22 the invariantmass distribution including the condition at least two tracks must reach the TOF is added. No efficiency or acceptance corrections are made yet.

5.7 Acceptance and efficiency corrections $\pi^+\pi^-\pi^+\pi^-$

In the same way the $\pi^+\pi^-$ invariant mass distribution needed to be corrected for acceptance and efficiency of the detector, the $\pi^+\pi^-\pi^+\pi^-$ distribution needs the same corrections, the same definitions apply for this case except that 4 track events are considered instead of two.

5.7.1 Simulation of ρ' mass distribution

The simulated proccess is $\rho(1720) \rightarrow \pi^+\pi^- + \rho^0 \rightarrow 4\pi$ anchored to runs 296244, 296273, 296304, 296377, 296510, 297193, 297218, 297481 and 297544. The decay mode was motivated by the invariant mass of the two pion subsystems shown in figure 5.20. In total 882 000 events were generated(≈100k

This thesis

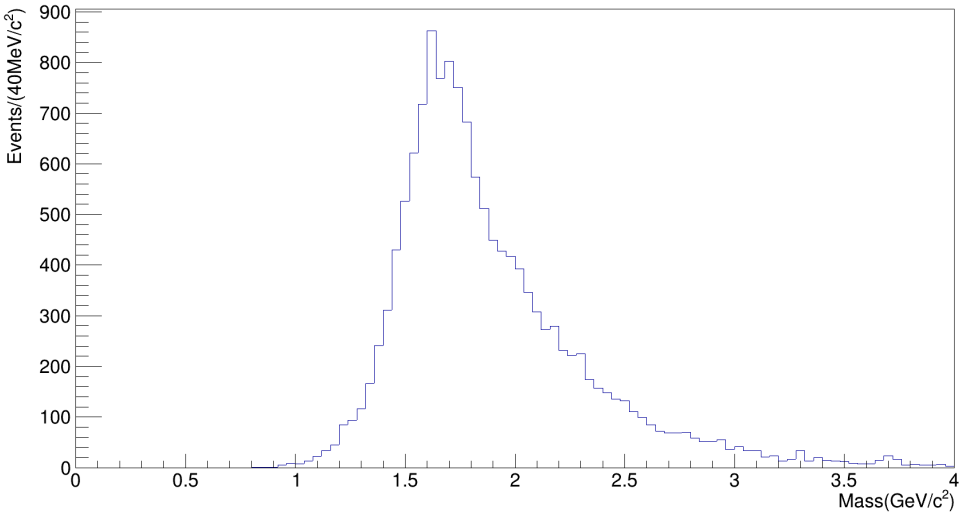

FIGURE 5.21: Reconstructed Invariant mass. Discussed in [33, 35]

This thesis

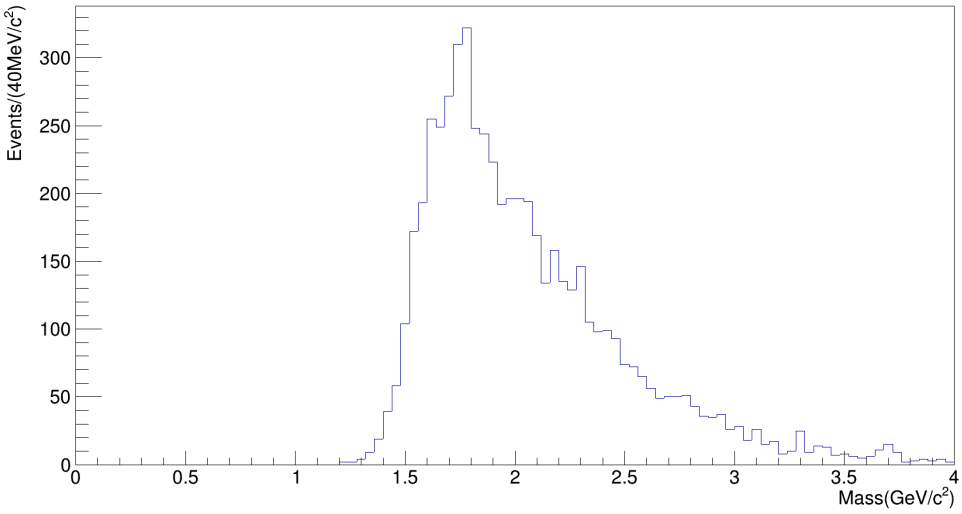

FIGURE 5.22: Reconstructed Invariant mass with at least two tracks reaching TOF. Discussed in [33, 35]

This thesis

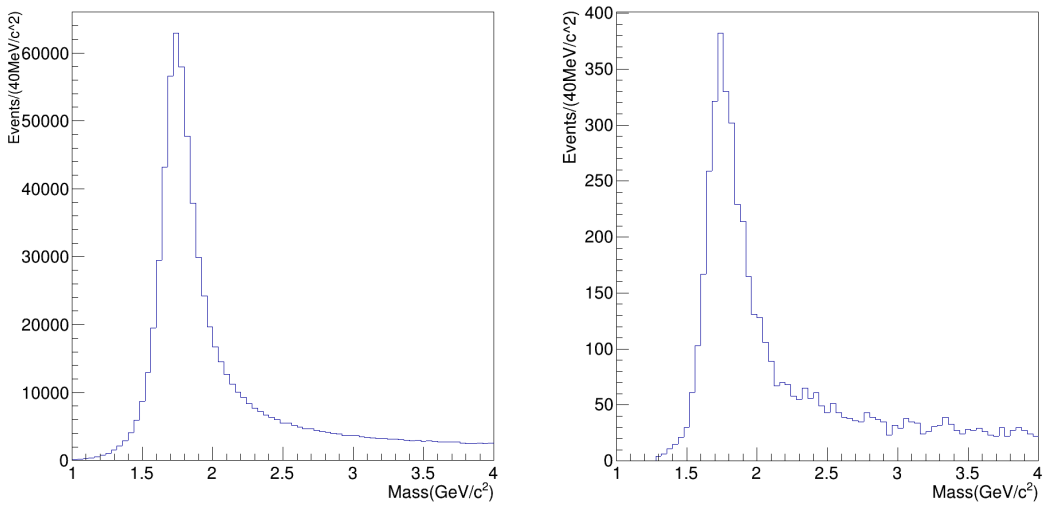

FIGURE 5.23: Generated (left) and reconstructed(right) invariant mass distributions. Discussed in [33, 32]

events per run). The rapidity region is restricted to $-1 \leq y \leq 1$, The angle distribution is uniform over all the azimuth. The ρ' maximum mass value is $5GeV/c^2$. The same analysis as for data is applied to the reconstructed events. The trigger conditions are the same as for the CCUP31 trigger, and as in the 2π case, information from simulated response of detectors is used to emulate the trigger. In figure 5.23 the invariant mass distributions for the generated and reconstructed ρ' invariant mass is shown for the anchored runs. The $Acc \times Eff$ calculated is shown in figure 5.24. Once again only tracks with momentum above $300MeV/c$ reach the TOF, so low momentum tracks are excluded.

The invariant mass distribution(figure 5.22), is corrected for acceptance and efficiency bin by bin. Because of the low efficiency, and therefore large errors, below $1.4GeV/c^2$ and above $2.3GeV/c^2$, only bins from $1.4GeV/c^2$ to $2.3GeV/c^2$ are corrected. The corrected invariant mass distributions can be seen in Figure 5.25

5.8 Xe-Xe Analysis

Xe-Xe collisions were carried out at ALICE in 2017 during the LHC17n period. A total of two runs were dedicated to this collision type: 280235 and 280234 runs. We present a brief study in 2 and 4 pions production. The same class AliAnalysisTaskUpcRho0 is used for the preselection, but the requirement that tracks have attached a TOF cluster is omitted. No specific trigger was required but information about the triggers activated was stored. Offline selection had the same requirements as for Pb-Pb, presented in section 5.3, except for the requirement in TOF cluster.

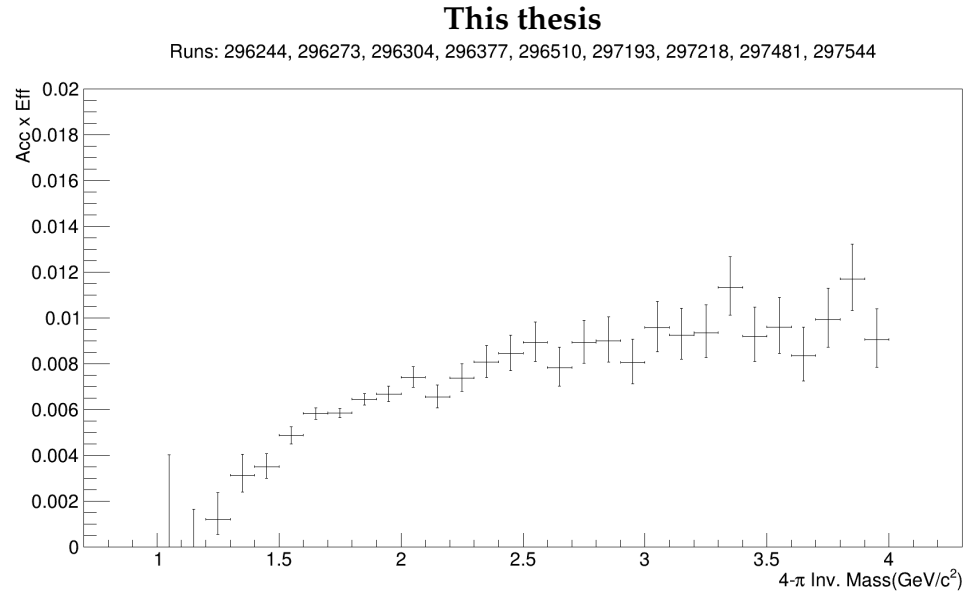

FIGURE 5.24: $Acc \times Eff$. Discussed in [32]

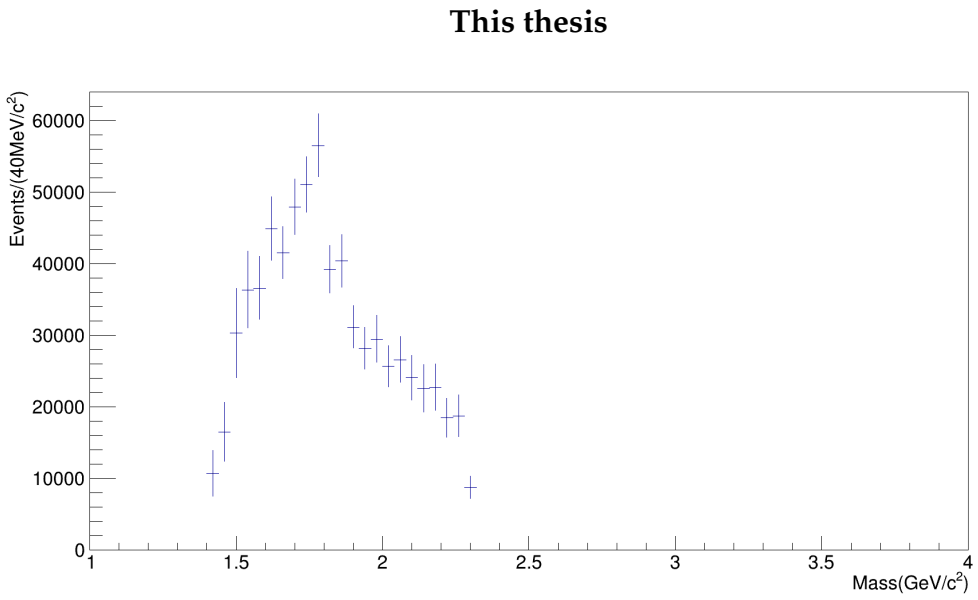

FIGURE 5.25: Invariant mass distribution (4-tracks) corrected for acceptance and efficiency

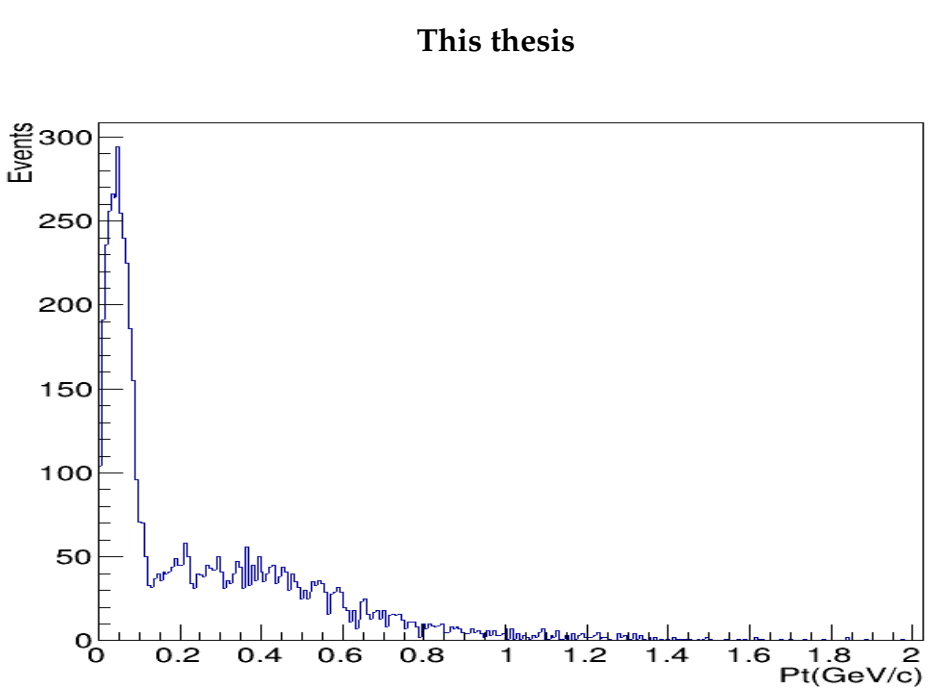

FIGURE 5.26: Transverse momentum distribution after all data cuts

5.8.1 $\pi^+\pi^-$ in Xe-Xe

A total of 38811 events were used. 2874 events remained after perform all the data cuts(PID,V0,AD,Pt,Vtx and rapidity cut). These events were triggered mainly by the trigger CCUP2 and CCUP25 which are defined as:

- CCUP2-B-NOPF-CENTNOTRD = *0VBA *0VBC 0OM2 0SH1
- CCUP25-B-NOPF-CENTNOTRD = *0VBA *0VBC 0STG 0OM2

The trigger elements were defined in section 7.2.1.

A detailed study for 2 pions in Xe-Xe collisions was performed by David Horak. A presentation and an analysis note can be found in:
https://indico.cern.ch/event/899086/

Only the invariant mass and the transverse momentum distribution are presented here, and can be seen in figures 5.26 and 5.27. Once again, for the transverse momentum a peak in the coherent region is observed. Also, for the mass distribution a peak is observed around the ρ^0 mass$\approx$ $775 MeV/c^2$, In figure 5.28 the invariant mass distribution obtained by David Horak in his analyses is shown. The invariant mass obtained in this thesis seems to agree with the one reported with David in shape and statistics.

5.8.2 $\pi^+\pi^-\pi^+\pi^-$ in Xe-Xe

For the 4 pions case 22561 events were used; 85 events remain after the data selection. In 79 of these events the trigger CCUP2 was activated and in 80 the trigger CCUP25 was activated. Similar plots as in Pb-Pb are displayed for Xe-Xe in figures 5.29 to 5.35.

This thesis

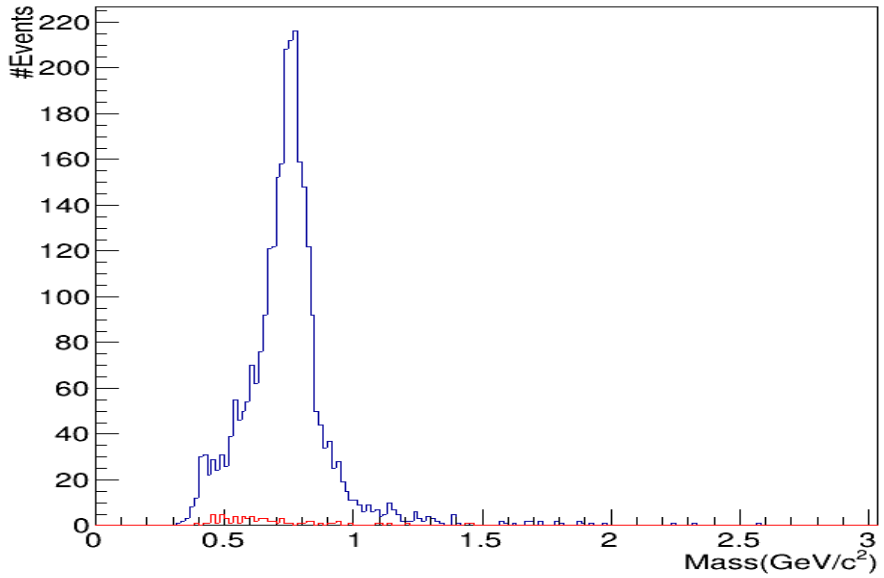

FIGURE 5.27: Invariant mass distribution after all data cuts

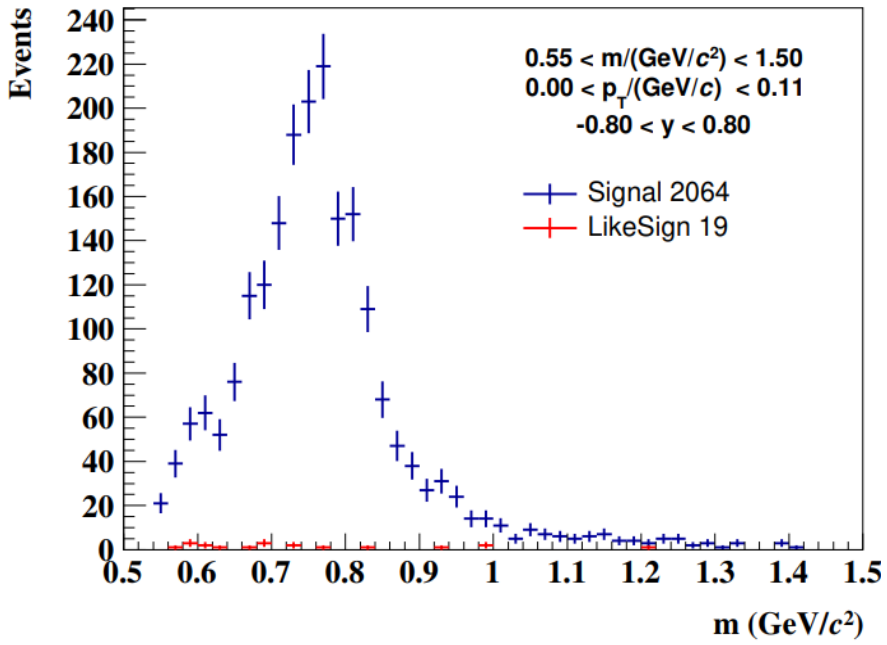

FIGURE 5.28: Invariant Mass distribution obtained by David Horak in his Analysis

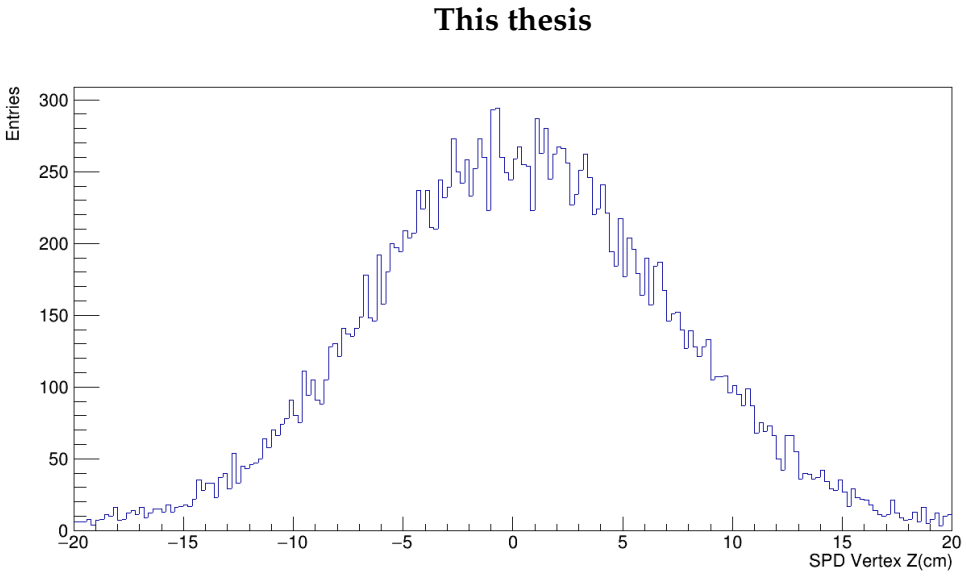

FIGURE 5.29: z vertex in Xe-Xe collision event

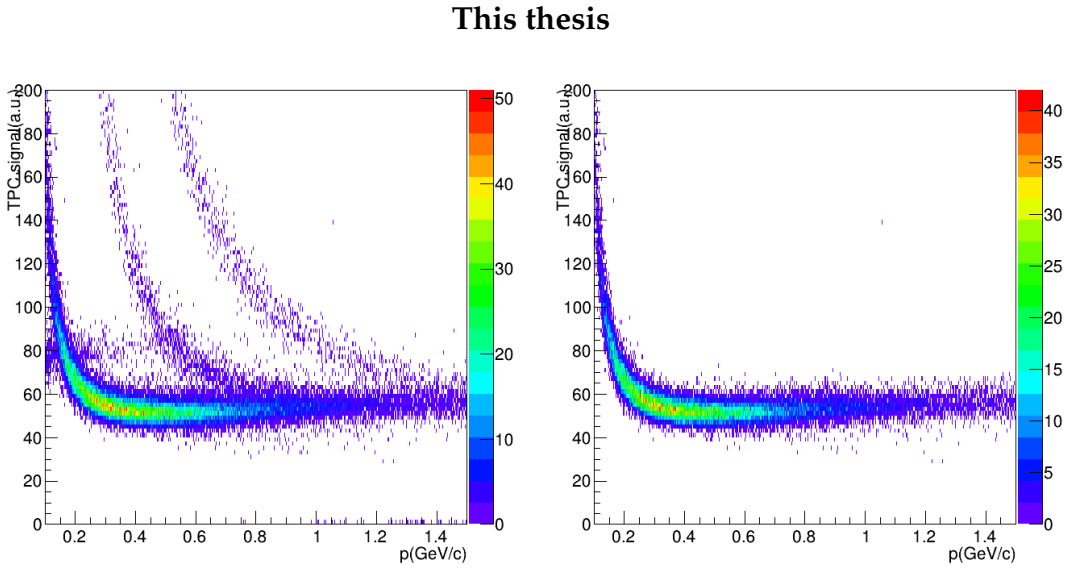

FIGURE 5.30: dE/dx vs momentum in Xe-Xe collisions, before PID cut (left), and after PID cut(right). Discussed in [34]

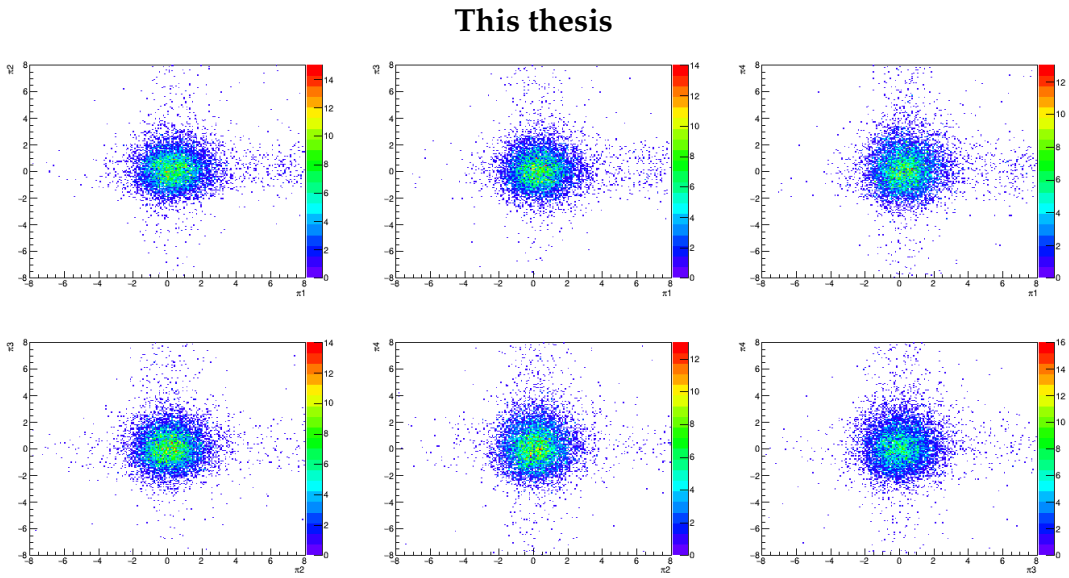

FIGURE 5.31: Correlation between the $\sigma's$ for the 4 tracks. Discussed in [34]

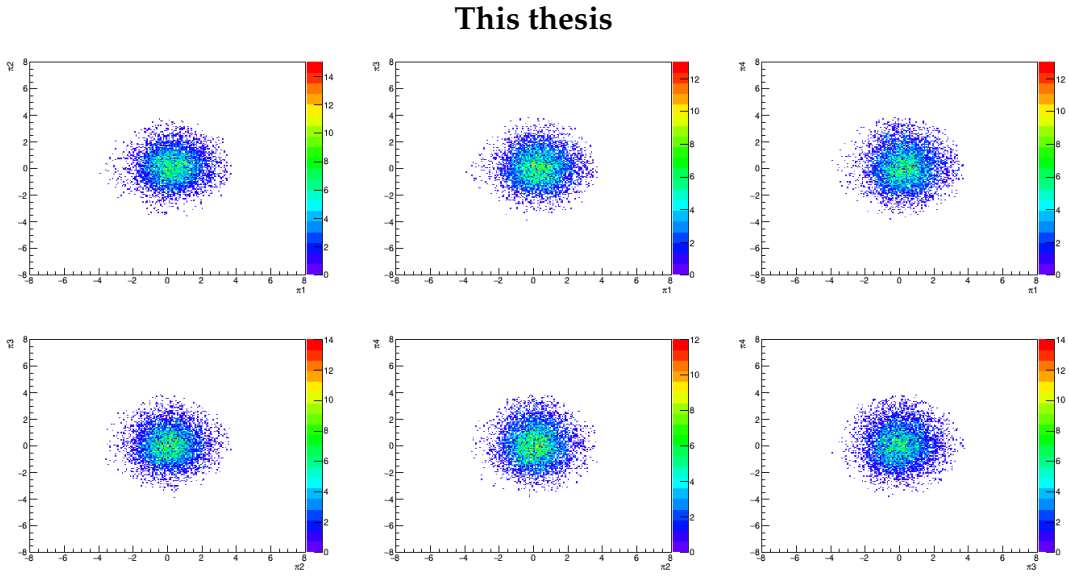

FIGURE 5.32: Correlation between the $\sigma's$ for the 4 tracks after PID cut. Discussed in [34]

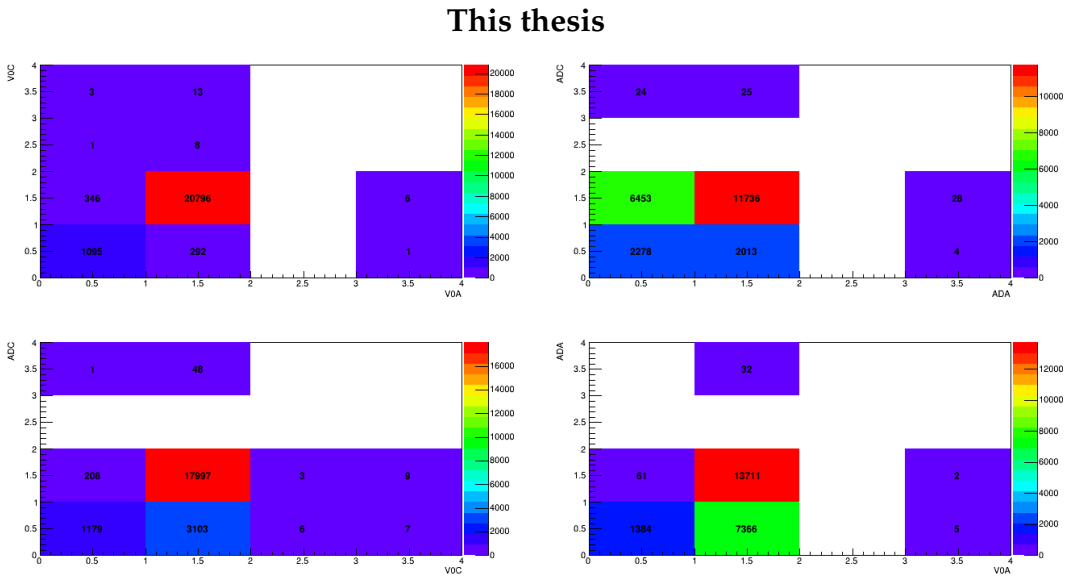

FIGURE 5.33: V0 and AD offline decisions. Discussed in [34]

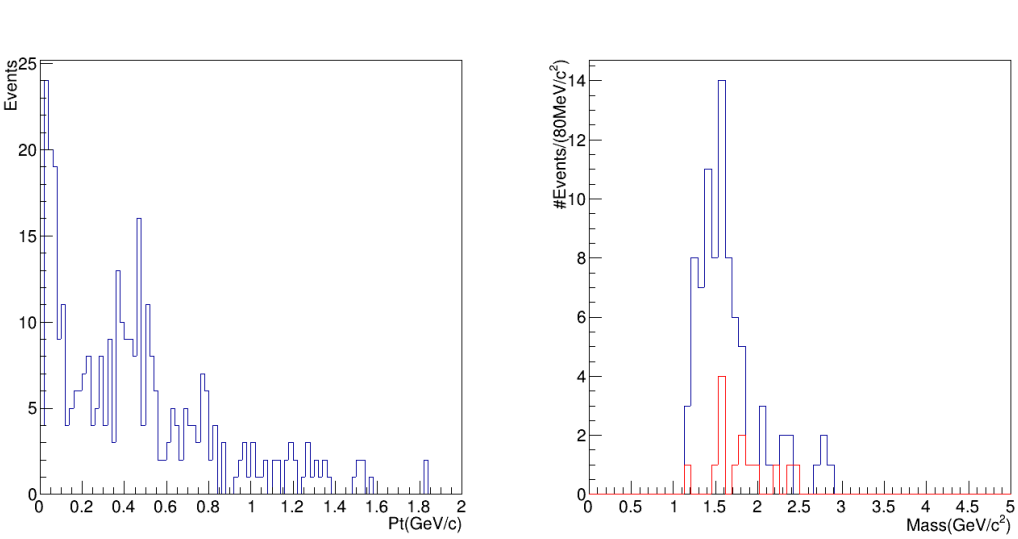

FIGURE 5.34: Transverse momentum after PID,V0,AD and ZN data cuts(left). Invariant mass after all data cuts(right); likesign distribution in red. Discussed in [34]

This thesis

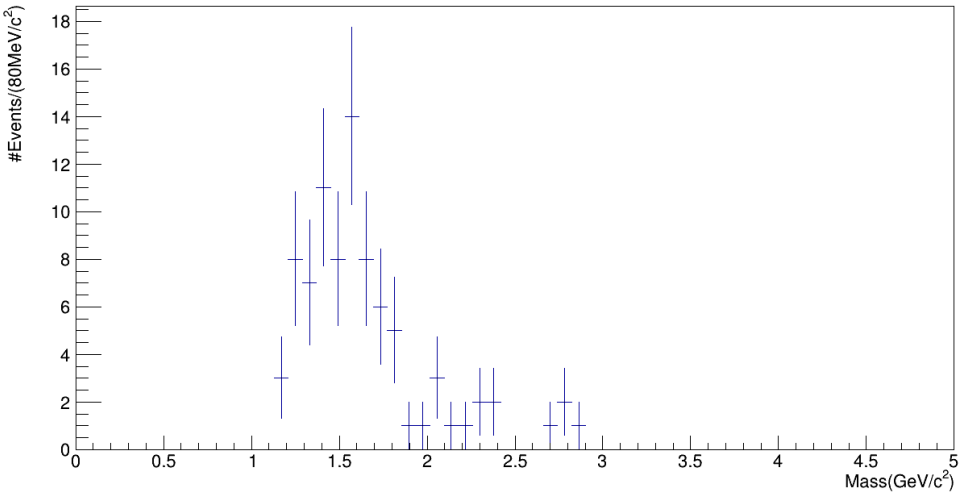

FIGURE 5.35: Invariant mass distribution. Discussed in [34]

Chapter 6

Conclusions

Data samples for Pb-Pb collisions during the year 2018 were analysed, the periods chosen were the LHC18r and the LHC18q. The trigger class selected was the CCUP31. The detectors used for the veto in the forward region of ALICE were V0 and AD; both are integrated as part of the mentioned trigger, and were also included as part of the data cuts.

For the 2 pions study a clear peak in the $\rho^0(775)$ mass region is seen, this result is in agreement with the reported previously by the STAR and the ALICE experiments for the photoproduction of the ρ^0. A peak in the mass region of the j/psi can also be seen, this could be muons background mainly, due to the peak is enhanced when the 2 tracks are required to reach the TOF, and as pointed out before, the TOF only measure particles with high momentum, and is harder to do accurately particle identification with high momentum particles using the TPC dE/dx, and especially between pions and muons due the expectations for dE/dx of both are quite similar.

For the 4 pions study, if the TOF condition is not required a peak that could correspond to the $\rho(1720)$ is seen around $1.6 GeV/c^2$, if the TOF requirement is applied the spectrum moves a bit to the high mass region, due to the high momentum pions that are required to reach TOF, the peak is located for this case about $1.8 GeV/c^2$. No peak is observed in the region of the $\rho(1450)$.

Acceptance and efficiency corrections were applied to both samples in Pb-Pb collisions. This value need to be calculated for the Xe-Xe sample.

Despite the low statistics in Xe-Xe a peak from coherent events in the uncorrected mass distribution is seen around $1.6 GeV/c^2$, in agreement with the 4 pions production study in STAR.

The invariant mass distributions still need to be fitted to some function (as for the results presented in chapter 2 for UPC in STAR and ALICE), in order to determine the ρ^0 and $\rho^{'}$ yield, the mass and width of each distribution.

Experimentally the cross section σ:

$$\sigma \propto \frac{(\text{Number of candidate events}) \times (\text{Branching ratio})}{Luminosity \times Acceptance \times Efficiency} \tag{6.1}$$

A further study that can be carried out is the determination of the cross section, for which the luminosity value need to be calculated, and also systematic errors for acceptance x efficiency value need to be determined.

The analysis and results exposed in this thesis have been presented and discussed in the PAG-UPC(ALICE expert's group in UPC) meetings [37, 38, 36, 35, 34, 33, 32]. and are included in an analysis note for the experiment[45].

Bibliography

[1] A. Baltz et al. "The Physics of Ultraperipheral Collisions at the LHC". In: *Phys.Rept.* (2008), pp. 1–171. URL: arXiv:0706.3356.

[2] D. Evans et al. *The ALICE Central Trigger System*. URL: http://www.ep.ph.bham.ac.uk/publications/bham-hep/05-02.pdf.

[3] J. Cabanillas et al. "ALICE Diffractive Detector Control System for RUN-II in the ALICE Experiment". In: (2016). URL: https://arxiv.org/abs/1609.08056.

[4] Tanabashi et al. "Review of Particle Physics". In: *Phys. Rev.* D98.030001 (2018). DOI: 10.1088/1674-1137/40/10/100001.

[5] Y. Zoccarato et al. "Front end electronics and first results of the ALICE V0 detector". In: *Nuclear Instruments and Methods in Physics Research A* (2010).

[6] ALICE Collaboration. "ALICE forward detectors: FMD, T0 and V0". In: *Technical design report* (). URL: http://cdsweb.cern.ch/record/781854..

[7] ALICE Collaboration. "The ALICE experiment at the CERN LHC". In: *JINST* (2008).

[8] C.A. Bertulani and G. Baur. "ELECTROMAGNETIC PROCESSES IN RELATIVISTIC HEAVY ION COLLISIONS". In: *Phys. Rep* 163 (1988), pp. 299–408.

[9] C.A. Bertulani and G. Baur. "Relativistic Heavy-Ion Physics Without Nuclear Contact". In: *Phys. Rep* 163-299 (1988).

[10] S. R. Klein C. A. Bertulani and J. Nystrand. "Physics of ultra-peripheral nuclear collisions". In: *Ann.Rev.Nucl.Part.Sci* 55 (2005), pp. 271–310. URL: arXiv:nucl-ex/0502005.

[11] J. Chwastowski. "Photoproduction at HERA". In: *Phys.Part.Nucl.* 35 (2004), pp. 619–632.

[12] ALICE Collaboration. *ALICE Technical Design Report of High–Level Trigger*. 2003. URL: https://wiki.kip.uni-heidelberg.de/ti/HLT/index.php/Design_%20Reports.

[13] ALICE Collaboration. "Coherent ρ^0 photoproduction in ultra-peripheral Pb–Pb collisions at $\sqrt{S_{NN}} = 2.76TeV$.". In: (). URL: arXiv:1503.09177%20[nucl-ex].

[14] CMS Collaboration. *Measurement of the inclusive 3-jet production differential cross section in proton-proton collisions at 7 TeV and determination of the strong coupling constant in the TeV range*. 2015. URL: https://arxiv.org/pdf/1412.1633.pdf.

[15] STAR Collaboration. "ρ^0 Photoproduction in AuAu Collisions at $\sqrt{S_{NN}} =$ 62.4GeV with STAR". In: (2008). URL: arXiv:1107.4630%20[nucl-ex]].

[16] STAR Collaboration. "ρ^0 Photoproduction in Ultra-Peripheral Relativistic Heavy Ion Collisions with STAR". In: *Phys.Rev.C77* (2008). URL: arXiv:0712.3320%20[nucl-ex].

[17] STAR Collaboration. "Coherent ρ^0 photoproduction in ultra-peripheral Pb–Pb collisions at $\sqrt{S_{NN}} = 2.76TeV$". In: *JHEP 09* (2015). URL: arXiv:1503.09177%20[nucl-ex].

[18] STAR Collaboration. "Coherent ρ^0 Production in Ultraperipheral Heavy-Ion Collisions". In: *Phys. Rev. Lett.* 89.27 (2002).

[19] STAR Collaboration. "Observation of $\pi^+\pi^-\pi^+\pi^-$Photoproduction in Ultra-Peripheral Heavy Ion Collisions". In: (). URL: arXiv:0912.0604%20[nucl-ex].

[20] STAR Collaboration. "Photoproduction in Ultra-Peripheral Relativistic Heavy Ion Collisions at STAR". In: (). URL: arXiv:0911.5219%20[nucl-ex].

[21] STAR Collaboration. "rho0 photoproduction in ultraperipheral relativistic heavy ion collisions at $\sqrt{S_{NN}} = 200GeV$". In: *Phys.Rev. C77* (2008). URL: arXiv:0712.3320%20[nucl-ex].

[22] CPEP. *Fundamental Particles and Interactions*. 2014. URL: http://www.cpepweb.org/images/2014-fund-chart.jpg.

[23] E. Daw. *Rapidity and Pseudorapidity*. 2012. URL: http://www.hep.shef.ac.uk/edaw/PHY206/Site/2012_course_files/phy206rlec7.pdf.

[24] G. Dellacasa et al. "ALICE technical design report of the inner tracking system (ITS)". In: (June 1999).

[25] G. Dellacasa et al. "ALICE technical design report of the time-of-flight system (TOF)". In: (Feb. 2000).

[26] G. Dellacasa et al. "ALICE: Technical design report of the time projection chamber". In: (Jan. 2000).

[27] E. Williams F. Weizsacker. In: *Z. Phys.* 88 (1934), p. 612.

[28] E. Fermi. "Zur Elektrodynamik bewegter Körper". In: *Annalen der Physik* 322.10 (1905), pp. 891–921. DOI: http://dx.doi.org/10.1002/andp.19053221004.

[29] V. Goncalves and M. Machado. "The QCD Pomeron in Ultraperipheral Heavy Ion Collisions: IV. Photonuclear Production of Vector Mesons". In: *Phys. J. C40,* (2005), p. 519.

[30] V. Goncalves and M. Machado. "Vector Meson Production in Coherent Hadronic Interactions: An update on predictions for RHIC and LHC". In: *Phys.Rev. C84* (2011). URL: arXiv:1106.3036%20[hep-ph].

[31] D Griffiths. *And introduction to elementary particle physics*. Morlenbach,Alemania: WILEY-VCH, 2004.

[32] *https://indico.cern.ch/event/899063/.*

[33] *https://indico.cern.ch/event/899085/.*

[34] *https://indico.cern.ch/event/899086/.*

[35] *https://indico.cern.ch/event/911888/.*

[36] *https://indico.cern.ch/event/911890/.*

[37] *https://indico.cern.ch/event/911902/.*

[38] *https://indico.cern.ch/event/911917/.*

[39] *https://starlight.hepforge.org/.*

[40] S. Klein and J. Nystrand. "Exclusive vector meson production in relativistic heavy ion collisions". In: *Phys.Rev. C60* (1999). URL: arXiv:hep-ph/9902259%20[hep-ph].

[41] M. Strikman L. Frankfurt and M. Zhalov. "Signals for black body limit in coherent ultraperipheral heavy ion collisions". In: *Phys.Lett. B537* (2002). URL: arXiv:hep-ph/0204175%20[hep-ph].

[42] M. Strikman M. Frankfurt and M. Zhalov. "Soft photoproduction physics". In: *Phys. Lett. B537* 51 (2002).

[43] V. Pozdnyakov. "Two-Photon Interactions at LEP". In: *Phys. Part. Nucl. Lett* 4 (2007), p. 289.

[44] M. H. Ross and L. Stodolsky. "Photon dissociation model for vector meson photoproduction". In: *Phys.Rev.* 149 (1996), pp. 1172–1181. URL: arXiv:hep-ph/0204175%20[hep-ph].

[45] *S. Paisano,Photoproduction of $\pi^+\pi^-$ and $\pi^+\pi^-\pi^+\pi^-$ in Pb-Pb collisions at ALICE-LHC; Analysis Note, website in progress.*

[46] Torbjörn Sjöstrand. "Soft photoproduction physics". In: *Phys. G: Nucl. Part.* 22 (1996), p. 709.

[47] P. Soding. "On the Apparent shift of the rho meson mass in photoproduction". In: *Phys.Lett.* 19 (1966), p. 702. URL: arXiv:1107.4630%20[nucl-ex]].

[48] *The ALICE Central Trigger Processor web site:* URL: http://epweb2.ph.bham.ac.uk/user/krivda/alice/.